

## Editor

**General Comment:** Dear Authors, The paper is accepted once you have addressed all the following minor revisions required by the reviewers. I report them below. Please, provide a revised manuscript and, if needed a point-to-point answer to them.

**Response:** Thanks for your effort to handle our submission.

We have carefully checked all the comments and made the corresponding revisions into the revised paper. In particular, Following the Reviewer #2's constructive comment, we divided the Section 3.4 into two parts for readability. These revisions made the revised paper clearer. Below please find our point to point response to your comments.

## Reviewer #1

**General Comment:** The authors have taken a very substantive redraft following the review process and adequately accounted for the vast majority of reviewer comments. The revised text is very much clearer and organized more logically which greatly aids readability. It is, to my opinion, unfortunate that the authors largely left the figures as they stood originally as I still find these figures very hard to decipher. That, ultimately is the authors' choice. I have a number of mainly minor comments detailed below.

**Response:** Thanks for your effort to evaluate our manuscript and high recommendation for the revised paper. As the other reviewer agree on the color use of the figures, we would like to keep their current form. Below please find our point to point response to your comments.

### Specific Comments:

1)

**Comment:** First, I wonder to what extent the results highlight inadequacy in reanalyses accounting for aerosol effects either via their omission, climatology, or even when applied (MERRA-2) if the direct and indirect effects are inadequately accounted for. It seems to me that a greater emphasis may be warranted in the discussion section in regard to whether the errors that appear to systematically affect several products may plausibly physically arise from inadequacies in the specification of and/or modelling of the impacts of aerosols. If the quantified errors are shown to be consistent with missing aerosol effects then that would be enormously helpful to point out more strongly to the reanalysis producers so they can perhaps undertake further experimentation and development work to rectify?

**Response:** Thanks for your comment.

Because of various assimilated observations, different forecast models and different assimilated methods in different reanalysis products, it's very difficult to quantify the presenting errors in regional warming from aerosol information errors in reanalyses. The result more advanced than previous studies is that "Comparing the  $T_a$  values from MERRA2 and MERRA shows that **MERRA2 displays improved performance over northern China**, as reflected by an increase in the correlation coefficient of 0.1 and a reduction in the RMSE of 0.1°C (Fig. 3)."

So, following the revision of Reviewer #2, we revised the sentence in Lines **694-697** in Section Discussion:

MERRA2's pioneering incorporation of time-varying aerosol loadings provides a way of improving the representation of regional temperature changes over regions **such as the North China Plain** where the impacts of aerosols on surface temperatures are significant.

2)

**Comment:** Lines 236-238 this wording isn't quite right. I think you intend something like "thus the inclusion of ERA-20CM in this study provides a useful benchmark series against which to ascertain the skill that is added via assimilation of various observations" or something like that?

**Response:** Thanks for your providing such information. Corrected as suggested: thus, the inclusion of ERA-20CM in this study provides a useful benchmark series against which to ascertain the skill that is added by assimilating various observations and to cognize the advantage of ensemble simulations.

3)

**Comment:** Line 273 impact of data inhomogeneities on (inhomogeneities and not homogenization here).

**Response:** Corrected as suggested.

4)

**Comment:** Line 426 Fig. 4 (Fig. to Figs.)

**Response:** Corrected as suggested.

## Reviewer #2

**General Comment:** I have read through the revised version of this paper. I thank the authors for taking note and responding to comments made in my original review. I recommend this version for publication, but do have the following specific comments on this version of the paper.

**Response:** Thanks for your high recommendation of our submission. Below please find our point to point response to your comments.

### Specific Comments:

1)

**Comment:** The Abstract and Conclusions identify welcome developmental steps involving incorporation of aerosol information and use of ensemble techniques. As pointed out in the body of the paper, the representations of  $T_a$  in ERA-Interim and JRA-55 are much better than those in other reanalyses, almost certainly in significant part due to their analysis of synoptic observations of the variable. This could be mentioned in the Abstract and Conclusions as another way the near-surface products of other reanalyses might be improved.

**Response:** Thanks for your providing such information, which is added in Abstract and Conclusions: In addition, the analysis of  $T_a$  observations helps representing regional warming in ERA-Interim and JRA-55.

2)

**Comment:** Table 1 has been tidied up following a comment in my original review, but the entry for ERA-20CM remains incorrect. The entry under "Assimilation System" for ERA-20CM has been changed from 4D-Var to 3D-Var, but this is still not right. There should be no entry under "Assimilation System" for ERA-20CM as it did not directly assimilate any atmospheric observations. Observations influence ERA-20CM only indirectly, through the forcing provided by CMIP5, and the prescribed SST, sea-ice and other model fields. ERA-20CM had no assimilation system of its own.

**Response:** We agree with the reviewer and deleted the "3D-Var" in the row of ERA-20CM.

3)

**Comment:** Regarding point (6) of my original review, I can accept the terminology "NWP-like reanalysis" and "climate reanalysis", even though I still do not particularly

like it. In Dee et al. (2014) – of which I am a co-author – we use the phrases “NWP-like reanalysis” and “extended climate reanalysis” which is subtly different, in that we (or at least I) regard the NWP-like reanalysis as one type of climate reanalysis and the extended climate reanalysis as another (longer) type. However, this slightly different nomenclature will not work in the present authors’ case as CFSR, which they classify as a climate analysis, is not “extended” in the sense used by Dee et al.

**Response:** Thanks for your comment. We provided an explanation in Lines 254-256: Note that the CFSR is classified into climate reanalysis in this study, mainly because it adopts a climate forecast system (Table 1).

4)

**Comment:** Line 229. It would probably be better to write “incorporate many observations” rather than “incorporate some observations”, even though the reanalyses have access to under 10% of the Chinese observations available to the authors. Globally, the number of observations used by ERA-Interim is some thirty thousand per day for the 1980s, and that number has risen considerably in recent years.

**Response:** Corrected as suggested.

5)

**Comment:** Lines 310 and 311. The sentence that spans these lines needs rephrasing as the correlation coefficient does not assess the absolute value.

**Response:** Corrected as “The bias, root mean squared error (*RMSE*) and standard deviation are used to assess the absolute value of  $T_a$ .”

6)

**Comment:** Line 359. “A homogeneous adjustment” should, I believe, be changed to “a homogenizing adjustment”.

**Response:** Corrected as suggested.

7)

**Comment:** Line 398. Delete “in ERA-Interim and JRA-55”.

**Response:** Corrected as suggested.

8)

**Comment:** Line 431. It would be better to replace “jointly determined” by “determined in part”, “determined to a significant extent” or some such phrasing. This is needed because surface air temperature is sensitive to a number of factors – such as circulation patterns and snow cover – that are not considered in the authors’ analysis, or only partially considered – a circulation anomaly may change  $T_a$  through differences in precipitation frequency that are taken into account, but may also change temperature due to advection. Similar qualifications are needed in several similar statements made in this and the following section.

**Response:** Following the reviewer’s suggestion, we replaced replace “jointly determined” by “determined in part”.

9)

**Comment:** Line 512. The trend in precipitation frequency is given in units of days/decade, implying that the precipitation frequency has a unit of days. How is precipitation frequency defined? Is it the number of days per month with appreciable rainfall? Maybe this is stated somewhere in the paper, but I do not recall seeing it.

**Response:** This information was revised in Lines **216-219**: Additionally, **precipitation frequency is defined as days in a year with daily precipitation at least 0.1 mm in this study**, which has been shown to provide a good indication of the effects of precipitation on the interannual variability and trends in  $T_a$  (Zhou et al., 2017).

10)

**Comment:** Page 527 and 528. Elsewhere the biases in temperature trends are related to biases in precipitation frequency,  $L_d$  etc.. But in this sentence it is the other way round. Is this a mistake?

**Response:** Yes, we have corrected it.

11)

**Comment:** Section 3.4 is a long one, and a more succinct synthesis of the results would probably help many readers.

**Response:** Thanks for your suggestions. We divided the original Section 3.4 into two parts, i.e., **1) The whole of China** and **2) Seven Subregions**. Accordingly, we adjusted the structure of this section for good readability.

12)

**Comment:** Line 578. Incorporating observations of Ta as done by ERA-Interim and JRA-55 is expected generally to reduce biases in the trends of analyses of Ta, not to introduce biases, as the reanalyses tend generally to reproduce the trends present in the observations, even in the presence of biases in the assimilating models. An exception can occur for regions where observations are not available for a substantial part of the time, particularly early or late in the period covered by the reanalysis. In this case, trends will be in error if the assimilating model has significant biases that are corrected at times when there are observations, but uncorrected when observations are absent.

**Response:** Thanks for your comment. We delete this sentence.

13)

**Comment:** Lines 617 and 618. Elevation differences can occur over time if stations are relocated, but this should be largely taken care of by the homogenization.

**Response:** Thanks for your comment. We delete this sentence.

14)

**Comment:** Lines 647 and 648. ERA-20CM should be referred to as ensemble simulation not ensemble forecasting.

**Response:** Corrected as suggested.

15)

**Comment:** Lines 663-670. It is stated that the comparison is for the reanalyses that do not incorporate observations, but ERA-Interim and JRA-55 are listed in the comparison. This needs amending.

**Response:** Thanks for your comment. We revised it in Lines **663-666**:

To provide a preliminary discussion of the improvements in climate forecast models in reflecting patterns in climate trends, **we compare the spatial patterns of the biases in the trends in  $R_s$ , precipitation frequency and  $L_d$  because observations of these variables are not included in the reanalyses.**

16)

**Comment:** Lines 691 and 691. This reads rather as if MERRA2 included time-vary aerosol loading in order to make a pioneering attempt to improve regional warming over the North China Plain. One suspects that the motivation for including time-varying aerosols in MERRA2 was much more general than this. The text could

be amended slightly to read something like “MERRA2’s pioneering incorporation of time-varying aerosol loadings provides a way of improving the representation of regional temperature changes over regions such as the North China Plain where the impacts of aerosols on surface temperatures are significant.”

**Response:** Thanks for your revision, which is added in Lines **694-697**:

MERRA2’s pioneering incorporation of time-varying aerosol loadings provides a way of improving the representation of regional temperature changes over regions such as the North China Plain where the impacts of aerosols on surface temperatures are significant.



# On the Suitability of Current Atmospheric Reanalyses for Regional Warming Studies over China

Chunlüe Zhou<sup>1</sup>, Yanyi He<sup>1</sup>, Kaicun Wang<sup>1\*</sup>

<sup>1</sup>College of Global Change and Earth System Science, Beijing Normal University,  
Beijing, 100875, China

**\*Corresponding Author:** Kaicun Wang, College of Global Change and Earth System  
Science, Beijing Normal University. Email: [kcwang@bnu.edu.cn](mailto:kcwang@bnu.edu.cn); tel.: +86  
(10)-58803143; fax: +86 (10)-58800059.

Submitted to *Atmospheric Chemistry and Physics*

~~March 22~~May 12, 2018

## Abstract

Reanalyses are widely used because they add value to routine observations by generating physically or dynamically consistent and spatiotemporally complete atmospheric fields. Existing studies include extensive discussions of the temporal suitability of reanalyses in studies of global change. This study adds to this existing work by investigating the suitability of reanalyses in studies of regional climate change, in which land-atmosphere interactions play a comparatively important role. In this study, surface air temperatures ( $T_a$ ) from 12 current reanalysis products are investigated; in particular, the spatial patterns of trends in  $T_a$  are examined using homogenized measurements of  $T_a$  made at ~2200 meteorological stations in China from 1979 to 2010. The results show that ~80% of the mean differences in  $T_a$  between the reanalyses and the *in situ* observations can be attributed to the differences in elevation between the stations and the model grids. Thus, the  $T_a$  climatologies display good skill, and these findings rebut previous reports of biases in  $T_a$ . However, the biases in the  $T_a$  trends in the reanalyses diverge spatially (standard deviation=0.15-0.30°C/decade using 1°×1° grid cells). The simulated biases in the trends in  $T_a$  correlate well with those of precipitation frequency, surface incident solar radiation ( $R_s$ ), and atmospheric downward longwave radiation ( $L_d$ ) among the reanalyses ( $r=-0.83$ ,  $0.80$  and  $0.77$ ;  $p<0.1$ ) when the spatial patterns of these variables are considered. The biases in the trends in  $T_a$  over southern China (on the order of -0.07°C/decade) are caused by biases in the trends in  $R_s$ ,  $L_d$  and precipitation frequency on the order of 0.10°C/decade, -0.08°C/decade, and -0.06°C/decade,

39 respectively. The biases in the trends in  $T_a$  over northern China (on the order of  
40  $-0.12^{\circ}\text{C}/\text{decade}$ ) result jointly from those in  $L_d$  and precipitation frequency. Therefore,  
41 improving the simulation of precipitation frequency and  $R_s$  helps to maximize the  
42 signal component corresponding to regional climate. In addition, [the analysis of  \$T\_a\$](#)   
43 [observations helps representing regional warming in ERA-Interim and JRA-55.](#)  
44 Incorporating vegetation dynamics in reanalyses and the use of accurate aerosol  
45 information, as in the Modern-Era Retrospective Analysis for Research and  
46 Applications, version 2 (MERRA-2), would lead to improvements in the modelling of  
47 regional warming. The use of the ensemble technique adopted in the  
48 twentieth-century atmospheric model ensemble ERA-20CM significantly narrows the  
49 uncertainties associated with regional warming in reanalyses (standard  
50 deviation= $0.15^{\circ}\text{C}/\text{decade}$ ).

## 1. Introduction

Observations and models are two fundamental approaches used in the understanding of climate change. Observations provide a direct link to the climate system via instruments, whereas models provide an indirect link and include information derived from measurements, prior knowledge and theory.

A large number of meteorological observations have been accumulated. These measurements, which are derived from a variety of sources, such as surface stations, ships, buoys, radiosondes, airplanes and satellites, record quantities that include near-surface and upper-air temperatures, humidity, wind and pressure. They constitute a major source of atmospheric information through the depth of the troposphere but suffer from incomplete spatiotemporal coverage and observation errors, including systematic, random and representation errors. Recent satellite-based observations have much better coverage; however, they suffer from other notable limitations, including temporal inhomogeneities (e.g., satellite drift) and retrieval errors (Bengtsson et al., 2007). These spatiotemporally varying gaps restrict the effective application of observations alone in climate research.

To fill in the gaps in observations, models are needed. Such models can be very simple; examples of simple models include linear interpolation or geo-statistical approaches that are based on the spatial and temporal autocorrelation of the observations. However, these models lack the necessary dynamical or physical mechanisms. Given the steady progress of numerical weather prediction (NWP) models in characterizing the global atmospheric circulation in the early 1980s (Bauer

et al., 2015), the first generation of reanalyses was produced by combining observations and dynamic models to provide the first global atmospheric datasets for use in scientific research (Bengtsson et al., 1982a, b).

After realizing the great value of this kind of reanalysis in atmospheric research, a step forward was taken with the suggestion made by Bengtsson and Shukla (1988) and Trenberth and Olson (1988) that most meteorological observations should be optimally assimilated under a fixed dynamical system over a period of time long enough to be useful for climate studies. In this way, available observations are ingested by advanced data assimilation techniques to provide a continuous initial state for an NWP model to produce the next short-term forecast. This procedure thus generates physically consistent and spatiotemporally complete three-dimensional atmospheric fields that are updated in light of observations.

Taking this suggestion as a guide, and given the improvements that have been made since the mid-1990s in the integrity of the observations, the models and the assimilation methods used, successive generations of atmospheric reanalyses established by several institutes have improved in quality. These reanalyses include the first two generations of global reanalyses produced by the National Centers for Environmental Prediction, NCEP-R1 (Kalnay et al., 1996) and NCEP-R2 (Kanamitsu et al., 2002) and the reanalyses produced by the European Centre for Medium-Range Weather Forecasts (ECMWF), ERA-15 (Gibson et al., 1997), ERA-40 (Uppala et al., 2005), and ERA-Interim (Dee et al., 2011b); the Japanese Meteorological Agency, JRA-25 (Onogi et al., 2007) and JRA-55 (Kobayashi et al., 2015); and the National

Aeronautics and Space Administration, the Modern-Era Retrospective Analysis for Research and Applications (MERRA) (Rienecker et al., 2011) and its updated version, MERRA-2 (Reichle et al., 2017).

These reanalyses produce global gridded datasets that cover multiple time scales and include a large variety of atmospheric, oceanic and land surface parameters, many of which are not easily or routinely observed but are dynamically constrained by large numbers of observations from multiple sources assimilated using fixed NWP models. During the data assimilation, prior information on uncertainties in the observations and models are used to perform quality checks, to derive bias adjustments and to assign proportional weights. Therefore, such reanalyses add value to the instrumental record through their inclusion of bias adjustments, their broadened spatiotemporal coverage and their increased dynamical integrity or consistency.

Previous studies have revealed that such reanalyses have contributed significantly to a more detailed and comprehensive understanding of the dynamics of the Earth's atmosphere (Dee et al., 2011b; Kalnay et al., 1996; Nguyen et al., 2013; Kidston et al., 2010; Simmonds and Keay, 2000; Simmons et al., 2010; Mitas and Clement, 2006). Extensive assessment studies have reported that most reanalyses display a certain level of performance in terms of their absolute values (Betts et al., 1996; Zhou and Wang, 2016b; Betts et al., 1998), interannual variability (Lin et al., 2014; Lindsay et al., 2014; Zhou and Wang, 2017a, 2016a; Wang and Zeng, 2012), distributions (Gervais et al., 2014; Heng et al., 2014; Mao et al., 2010) and relationships among variables (Niznik and Lintner, 2013; Cash et al., 2015; Zhou et al., 2017; Zhou and Wang,

2016b;Betts, 2004) over regions worldwide. However, these aspects of reanalyses still contain certain errors that restrict the general use of reanalyses, especially in climate applications.

The errors displayed by reanalysis products arise from three sources: observation error, model error and assimilation error (Thorne and Vose, 2010;Parker, 2016;Lahoz and Schneider, 2014;Dee et al., 2014;Zhou et al., 2017). Specifically, observation error incorporates systematic and random errors in instruments and their replacements, errors in data reprocessing and representation error, which arises due to the spatiotemporal incompleteness of observations (Dee and Uppala, 2009;Desroziers et al., 2005). Model error refers mainly to the inadequate representation of physical processes in NWP models (Peña and Toth, 2014;Bengtsson et al., 2007), such as the lack of time-varying surface conditions, such as vegetation growth (Zhou and Wang, 2016b;Trigo et al., 2015), and incomplete cloud-precipitation-radiation parameterizations (Fujiwara et al., 2017;Dolinar et al., 2016). Assimilation error describes errors that arise in the mapping of the model space to the observation space and errors in the topologies of cost functions (Dee, 2005;Dee and Da Silva, 1998;Lahoz and Schneider, 2014;Parker, 2016).

These reanalyses mentioned above consist of the true climate signal and the nonlinear interactions among the observation error, the model error, and the assimilation error that arise during the assimilation process. These time-varying errors can introduce spurious trends without being eliminated by data assimilation systems. Many spurious variations in climate signals were also identified in the

early-generation reanalyses (Bengtsson et al., 2004;Andersson et al., 2005;Chen et al., 2008;Zhou and Wang, 2016a, 2017a;Zhou et al., 2017;Schoeberl et al., 2012;Xu and Powell, 2011;Hines et al., 2000;Cornes and Jones, 2013). Therefore, reanalyses produced using the existing reanalysis strategy may not accurately capture climate trends (Trenberth et al., 2008), even though they may contain relatively accurate estimates of synoptic or interannual variations in the Earth's atmosphere.

An emerging requirement for climate applications of reanalysis data is the accurate representation of decadal variability, further increasing the confidence in the estimation of climate trends. This kind of climate reanalysis is required to be free, to a great extent, from other spurious non-climatic signals introduced by changing observations, model imperfections and assimilation error; that is, they must maintain temporal consistency. Therefore, the extent to which climate trends can be assessed using reanalyses attracts much attention and sparks heated debates (Thorne and Vose, 2010;Dee et al., 2011a;Dee et al., 2014;Bengtsson et al., 2007).

Given the great progress that has been made in climate forecasting models (which provide more accurate representations of climate change and variability) and coupled data assimilation, many efforts have been made by several institutes to build consistent climate reanalyses using the strategy of assimilating a relatively small number of high-quality long-term observational datasets. The climate reanalyses of this new generation extend back to the late nineteenth century and include the Climate Forecast System Reanalysis (CFSR), which is produced by the National Centers for Environmental Prediction (Saha et al., 2010); NOAA 20CRv2c, which is produced by



the University of Colorado's Cooperative Institute for Research in Environmental Sciences (CIRES) in cooperation with the National Oceanic and Atmospheric Agency (NOAA) (Compo et al., 2011); and ERA-20C (Poli et al., 2016), ERA-20CM (Hersbach et al., 2015) and CERA-20C (Laloyaux et al., 2016), which are produced by the ECMWF. Compo et al. (2013) suggested that the NOAA 20CRv2c reanalysis can reproduce the trend in global mean surface air temperatures. In addition, the uncertainties estimated from multiple ensembles are provided to increase the confidence of the climate trends (Thorne and Vose, 2010; Dee et al., 2014).

From NWP-like reanalyses to climate reanalyses, existing studies focus mainly on comparing the differences in temporal variability between the reanalyses and observations using some statistical metrics, e.g., the mean values, standard deviations, interannual correlations, probability density functions and trends of surface air temperature over regions worldwide. These evaluations provide insight into the temporal evolution of the Earth's atmosphere. However, they lack the performance evaluations used in reanalyses in representing the spatial patterns of these statistics associated with the role of the coupled land-atmosphere and dynamical processes of the climate system. Moreover, the assessment of these spatial patterns provides a direct means of examining the most prominent advantage of reanalyses over geo-statistical interpolation; thus, the spatial patterns require comprehensive investigation.

This study employs high-density station-based datasets of quantities including surface air temperatures ( $T_a$ ), the surface incident solar radiation ( $R_s$ ), the surface

downward longwave radiation ( $L_d$ ), and precipitation measured at ~2200 meteorological stations within China from 1979 to 2010. It provides a quantitative examination of the simulated patterns of variations in  $T_a$  in both the NWP-like and climate reanalyses and considers the climatology, the interannual variability, the mutual relationships among relevant quantities, the long-term trends and their controlling factors. The results indicate the strengths and weaknesses of the current reanalyses when applied in regional climate change studies and provide possible ways to improve these reanalyses in the near future.

## **2. Data and Methods**

### **2.1 Observational Datasets**

The latest comprehensive daily dataset (which contains averages at 0, 6, 12, and 18 UTC) of quantities that include  $T_a$ , precipitation, sunshine duration, relative humidity, water vapor pressure, surface pressure and the cloud fraction from approximately 2400 meteorological stations in China from 1961 to 2014, of which only approximately 194 participate in global exchanges, is obtained from the China Meteorological Administration (CMA; <http://data.cma.cn/data>). Approximately 2200 stations with complete and homogeneous data are selected for use in this study (Wang and Feng, 2013; Wang, 2008; Wang et al., 2007). The high density of meteorological stations in China promotes the representation of regional patterns in surface warming by reanalyses and the assessment of the skill of simulations.

$R_s$  values based on the revised Ångström-Prescott equation (Wang et al.,

205 2015;Yang et al., 2006;Wang, 2014) are used in this study. The derived  $R_s$  values  
 206 consider the effects of Rayleigh scattering, water vapor absorption and ozone  
 207 absorption (Wang et al., 2015;Yang et al., 2006) and can accurately reflect the effects  
 208 of aerosols and clouds on  $R_s$  over China (Wang et al., 2012;Tang et al., 2011). Several  
 209 intensive studies have reported that the derived  $R_s$  values can accurately depict the  
 210 interannual, decadal and long-term variations in  $R_s$  (Wang et al., 2015;Wang,  
 211 2014;Wang et al., 2012).

212  $L_d$  is typically estimated by first determining the clear-sky radiation and  
 213 atmospheric emissivity (Brunt, 1932;Choi et al., 2008;Bilbao and De Miguel, 2007),  
 214 and then correcting for the cloud fraction (Wang and Liang, 2009;Wang and  
 215 Dickinson, 2013). The derived  $L_d$  values can directly reflect the greenhouse effect of  
 216 atmospheric water vapor and clouds. Additionally, ~~a precipitation event~~[precipitation](#)  
 217 [frequency](#) is defined as [days in a year with](#) daily precipitation ~~of~~ at least 0.1 mm in  
 218 this study, which has been shown to provide a good indication of the effects of  
 219 precipitation on the interannual variability and trends in  $T_a$  (Zhou et al., 2017). Taken  
 220 together, the derived  $R_s$  and  $L_d$  values are able to physically quantify the effects of  
 221 solar radiation and the greenhouse effect on surface warming. Precipitation frequency  
 222 can regulate the partitioning of available energy into latent and sensible heat fluxes  
 223 and thus modulates the variations in  $T_a$  (Zhou et al., 2017;Zhou and Wang, 2017a).

## 224 2.2 Reanalysis Products

225 All of the major global atmospheric reanalysis products are included in this study  
 226 (Table 1). The reanalyses are summarized below in terms of three aspects, i.e., the

observations assimilated and the forecast model and assimilation method used. The  
 NWP-like reanalyses assimilate many conventional and satellite datasets from  
 multiple sources (Table 1) to characterize the basic upper-air atmospheric fields; the  
 spatiotemporal errors of these datasets vary with time. In particular, the ERA-Interim  
 and JRA-55 reanalyses incorporate ~~some~~ many observations of  $T_a$ , and the MERRA2  
 reanalysis includes aerosol optical depth estimates from satellite retrievals and model  
 simulations based on emission inventories, whereas most of the other reanalyses use  
 climatological aerosols (Table 1). To derive consistent long-term climate signals, the  
 new strategy adopted by climate reanalyses involves the assimilation of a small  
 number of relatively effective observed variables, e.g., surface pressure (Table 1).  
 Except for its lack of the assimilation of surface pressure, ERA-20CM employs the  
 same forecast model and external forcings as ERA-20C (Table 1); ~~thus, the inclusion~~  
~~of ERA-20CM in this study will provide insight into the suitability of current~~  
~~atmospheric reanalyses in studies of regional warming~~thus, the inclusion of  
ERA-20CM in this study provides a useful benchmark series against which to  
ascertain the skill that is added by assimilating various observations and to cognize  
the advantage of ensemble simulations. The reanalyses adopt different sea surface  
 temperatures (SSTs) and sea ice concentrations for different time periods, which may  
 lead to temporal discontinuities in the climate signals derived from the reanalyses  
 (Table 1). To address this issue, the boundary conditions in CFSR are derived from its  
 coupled ocean-sea ice models instead of observations (Table 1). CFSR, NOAA  
 20CRv2c and NOAA 20CRv2 use monthly greenhouse gases (GHGs) with annual

means near those used in CMIP5. On the other hand, in ERA-Interim, the GHGs increase more slowly than in CMIP5 after 2000. Finally, NCEP-R1 and NCEP-R2 adopt constant global mean concentrations of the GHGs (Table 1).

The forecast model is a fundamental component of a reanalysis that provides the background fields to the assimilation system. Different reanalyses produced by a single institute generally use similar physical parameterizations; however, updated versions of these parameterizations and higher spatial resolutions are used in the newer generations of these realizations (Table 1). [Note that the CFSR is classified into climate reanalysis in this study, mainly because it adopts a climate forecast system \(Table 1\).](#) The assimilation methods adopted by the current reanalyses incorporate variational methods (3D-Var and 4D-Var) and the ensemble Kalman filter (EnKF) approach (Table 1).

The 2-m  $T_a$  in NCEP-1, NCEP-2, MERRA, MERRA-2, ERA-20C, ERA-20CM, CERA-20C, NOAA 20CRv2c, NOAA 20CRv2 and CFSR are model-derived fields that are functions of the surface skin temperature, the temperature at the lowest model level, the vertical stability and the surface roughness, which are constrained primarily by observations of upper-air variables and the surface pressure (Kanamitsu et al., 2002; Rienecker et al., 2011; Reichle et al., 2017; Poli et al., 2016; Hersbach et al., 2015; Laloyaux et al., 2016; Compo et al., 2011; Saha et al., 2010). However, the  $T_a$  in ERA-Interim and JRA-55 are post-processing products by a relatively simple analysis scheme between the lowest model level and the surface and are analysed using ground-based observations of  $T_a$ , with the help of Monin-Obukhov similarity profiles

consistent with the model's parameterization of the surface layer (Dee et al., 2011b; Kobayashi et al., 2015). Additionally, radiation calculations are diagnostically determined from the prognostic cloud condensate microphysics parameterization, and the cloud macrophysics parameterization assumes a maximum-random cloud overlapping scheme (Saha et al., 2010; Dolinar et al., 2016).

### 2.3 Method Used to Homogenize the Observed Time Series

Problems related to the observational infrastructure (e.g., instrument ageing and changes in observing practices) and station relocations can also lead to false temporal heterogeneity in time series. Therefore, it is necessary to diminish the impact of data inhomogeneities on the trends in the observed variables during the study period of 1979-2010.

We use the RHtestsV4 software package (Wang and Feng, 2013) to detect and homogenize the breakpoints in the monthly time series. The package includes two algorithms. Specifically, the PMFred algorithm is based on the penalized maximal  $F$ -test ( $PMF$ ) without a reference series (Wang, 2008), and the PMTred algorithm is based on the penalized maximal  $t$ -test ( $PMT$ ) with a reference series (Wang et al., 2007).

In this study, we first use the PMFred algorithm to identify potential reference series at the 95% significance level. We then reconstruct homogenous series for each inhomogeneous series using the following steps: 1) horizontal and vertical distances from the inhomogeneous station of less than 110 km and 500 m, respectively, are specified; 2) correlation coefficients between the first-order difference in the

homogeneous series with that in the inhomogeneous one exceeding 0.9 are required; and 3) the first ten homogeneous series are averaged using inverse distance weighting to produce a reference series for the inhomogeneous station. Finally, we apply the PMTred algorithm to test all of the inhomogeneous series using the nearby reference series. Several intensive studies have been conducted that indicate the PMTred algorithm displays good performance in detecting change points in inhomogeneous series (Venema et al., 2012; Wang et al., 2007).

If a breakpoint is found to be statistically significant, the quantile-matching (QM) adjustment in RHtestsV4 is recommended for making adjustments to the time series (Wang et al., 2010; Wang and Feng, 2013); in such cases, the longest available segment from 1979 to 2010 is used as the base segment. The QM adjustment aims to match the empirical distributions from all of the detrended segments with that of the specific base segment (Wang et al., 2010). In addition, we replicate the procedures above for the sparsely distributed stations over western China and the Tibetan Plateau. The PMTred algorithm and the QM adjustment have recently been used successfully to homogenize climatic time series (Aarnes et al., 2015; Tsidu, 2012; Dai et al., 2011; Siswanto et al., 2015; Wang and Wang, 2016; Zhou et al., 2017).

As such, the significant breakpoints are detected and adjusted at a confidence level of 95% at 1092 of the 2193 (49.8%) stations for the  $T_a$  time series; 1079 of the 2193 (49.2%) stations for the  $R_s$  time series; 64 of the 2193 (2.9%) stations for precipitation frequency time series; 971 of the 2193 (44.2%) stations for the  $L_d$  time series; 944 of the 2193 (43.0%) stations for the water vapor pressure time series; and

956 of the 2193 (43.6%) stations for the cloud fraction time series.

## 2.4 Trend Calculations, Partial Linear Regression, and Total Least Squares

The bias, root mean squared error (*RMSE*) ~~and~~, standard deviation ~~and correlation coefficient ( $r$ )~~ are used to assess the absolute value of  $T_a$ .—The trends in  $T_a$  and the relevant variables are calculated using the ordinary least squares method (OLS) and the two-tailed Student's  $t$ -test. To determine whether the reanalyses contain biases in these trends, the two-tailed Student's  $t$ -test is also applied to the differences in the time series between the reanalyses and the homogeneous observations.

The partial least squares approach is used to investigate the net relationship between the detrended  $T_a$  values and the relevant variables ( $R_s$ ,  $L_d$  and precipitation frequency) after statistically excluding the confounding effects among the relevant variables (Zhou et al., 2017). To evaluate the potential collinearity of independent variables in the regression model, the variance inflation factor (*VIF*) is calculated. The *VIFs* for  $R_s$ , precipitation frequency and  $L_d$  are less than 4. Specifically, the *VIF* for China of 2.19 is much less than the threshold of 10, above which the collinearity of regression models is bound to adversely affect the regression results (Ryan, 2008).

The Pearson correlation coefficient ( $r$ ) is used to reveal the spatial relationship between  $T_a$  and the relevant variables. To further investigate the relationship between the spatial distributions of the biases in the trends in  $T_a$  and the relevant parameters among the twelve reanalysis products, the weighted total least squares (WTLS) is adopted, in which the spatial standard deviations and correlations of pairs of variables on  $1^\circ \times 1^\circ$  grid cells are included (Reed, 1989; York et al., 2004; Golub and Van Loan,



1980;Hyk and Stojek, 2013;Tellinghuisen, 2010):

$$\omega(x_i) = 1/\hat{\sigma}_{x_i}^2 \quad (1)$$

$$\omega(y_i) = 1/\hat{\sigma}_{y_i}^2 \quad (2)$$

$$W_i = \frac{\omega(x_i) \cdot \omega(y_i)}{\omega(x_i) + b^2 \omega(y_i) - 2b \cdot r_i \sqrt{\omega(x_i) \cdot \omega(y_i)}} \quad (3)$$

$$U_i = x_i - \sum_i^n (W_i \cdot x_i) / \sum_i^n (W_i) \quad (4)$$

$$V_i = y_i - \sum_i^n (W_i \cdot y_i) / \sum_i^n (W_i) \quad (5)$$

$$\beta_i = W_i \left[ \frac{U_i}{\omega(y_i)} + \frac{b \cdot V_i}{\omega(x_i)} - (b \cdot U_i + V_i) \frac{r_i}{\sqrt{\omega(x_i) \cdot \omega(y_i)}} \right] \quad (6)$$

$$b = \frac{\sum_{i=1}^n W_i \cdot \beta_i \cdot V_i}{\sum_{i=1}^n W_i \cdot \beta_i \cdot U_i} \quad (7)$$

where  $x_i$  and  $y_i$  are the median trends in  $x$  and  $y$  (e.g.,  $T_a$  and  $R_s$ ) for the  $i^{th}$  reanalysis product;  $\hat{\sigma}_{x_i}$ ,  $\hat{\sigma}_{y_i}$  and  $r_i$  are the spatial standard deviations and correlations of the trends in  $x$  and  $y$  for the  $i^{th}$  reanalysis product;  $\beta_i$  is the least squares-adjusted value;  $W_i$  is the weight of the residual error; and  $b$  is the slope estimated by iterative methods with a relative tolerance of  $10^{-16}$ .

The Monte Carlo method with 10000 experiments is applied to estimate the 90% confidence intervals of the slope  $b$ . In the Monte Carlo method, the grid index for the  $1^\circ \times 1^\circ$  grid cells over China, which ranges from 1 to 691, is generated as a random number. On this basis, we can sample the spatial pattern in the biases in the trends in  $T_a$ ,  $R_s$ ,  $L_d$  and precipitation frequency. We then calculate the median trends and their spatial standard deviations and correlations for each experiment used in the WTLS.

### 3. Results

#### 3.1 Dependency of Surface Air Temperature Differences on Elevation Differences

Fig. 1 illustrates the differences in  $T_a$  from the NWP-like reanalyses and climate reanalyses relative to the homogenized station-based observations over China during the period of 1979-2010. When the  $T_a$  values measured at the stations are compared directly with those in the corresponding model grid cells, the results indicate that the reanalysis products underestimate  $T_a$  over most of the regions in China (by  $-0.28^{\circ}\text{C}$  to  $-2.56^{\circ}\text{C}$ ). These discrepancies are especially pronounced over the Tibetan Plateau and Middle China, where the underestimation ranges from  $-2.75^{\circ}\text{C}$  to  $-7.00^{\circ}\text{C}$  and from  $-1.19^{\circ}\text{C}$  to  $-2.91^{\circ}\text{C}$ , respectively (Fig. 1 and Table 2). A [homogenizinghomogeneous](#) adjustment of  $0.03^{\circ}\text{C}$  from the raw  $T_a$  observations is insufficient to cancel the underestimation of  $T_a$  by the reanalyses (Fig. 1 and Table 2). Similar biases in  $T_a$  within various regions worldwide have been widely reported by previous studies (Mao et al., 2010; Pitman and Perkins, 2009; Reuten et al., 2011; Wang and Zeng, 2012; Zhou et al., 2017; Zhou and Wang, 2016b).

However, we found that the spatial patterns in the differences in  $T_a$  are well correlated with the elevation differences between models and stations, as reflected by correlation coefficients ( $r$ ) of 0.85 to 0.94 (Figs. 2 and S1). These results are in accordance with the reports from NCEP-R1, NCEP-R2 and ERA-40 (You et al., 2010; Ma et al., 2008; Zhao et al., 2008). The elevation differences ( $\Delta\text{Height}$ ; Figs. 2 and S1) between the stations and the model grids consists of the filtering error in the

elevations used in the spectral models ( $\Delta f$ ) and differences in the site-to-grid elevations ( $\Delta s$ ) due to the complexity of the orographic topography. We further quantify the relative contributions of these factors to the  $T_a$  differences. The elevation differences can explain approximately 80% of the  $T_a$  differences; approximately 74% is produced by the site-to-grid elevation differences, and approximately 6% is produced by the filtering error in the elevations used in the spectral models (Fig. 2).

The regression coefficient of the differences in  $T_a$  is approximately  $6^{\circ}\text{C}/1\text{ km}$ , which is similar to the lapse rate at the surface (Fig. 2). Lapse rate values that exceed  $6^{\circ}\text{C}/1\text{ km}$  can be seen over the Tibetan Plateau (shown as red dots in Fig. 2). This result is very consistent with the reported lapse rates over China (Li et al., 2015; Fang and Yoda, 1988). In addition, the rate of decrease in the model filtering error is approximately  $4^{\circ}\text{C}/1\text{ km}$  among the twelve reanalyses (Fig. 2). These results have important implications for the skill of the simulated  $T_a$  climatologies of the twelve reanalyses over China.

### 3.2 Comparison of Regional-scale Surface Air Temperature Series

Fig. 3 shows Taylor diagrams of annual  $T_a$  anomalies from the observations and reanalyses over China and its seven subregions. We find that the correlations between the annual  $T_a$  anomalies in the twelve reanalysis products and the observations are reasonably strong, as reflected by a median  $r$  of 0.95 (Fig. 3), despite the relatively weak correlations over the Tibetan Plateau associated with NCEP-R2 ( $r=0.24$ ) and CFSR ( $r=0.53$ ). The simulated time series of  $T_a$  anomalies over eastern China are depicted most accurately by the reanalyses (Fig. 3c-g).

Overall, the NWP-like reanalyses (denoted by numbers 3-7) display better skill than the climate reanalyses (denoted by numbers 8-14) in this regard (Fig. 3). ERA-Interim and JRA-55 display the best performance in the simulated time series of  $T_a$  anomalies over China ( $r=1.00$ ,  $RMSE=0.05^{\circ}C$ ) and the seven regions ( $r=0.98$ ,  $RMSE=0.1^{\circ}C$ ) (Fig. 3), perhaps due to their analysis of surface air temperature observations [in ERA-Interim and JRA-55](#) (Table 1).

Comparing the  $T_a$  values from MERRA2 and MERRA shows that MERRA2 displays improved performance over northern China, as reflected by an increase in the correlation coefficient of 0.1 and a reduction in the RMSE of  $0.1^{\circ}C$  (Fig. 3). This result may occur because MERRA2 includes time-varying aerosol loadings (Balsamo et al., 2015; Reichle et al., 2011). However, the incorporation of this information does not improve the results over Southeast China (Fig. 3h).

CERA-20C displays better performance than ERA-20C and ERA-20CM, perhaps related to the inclusion of coupled climate forecast models and data assimilation, as well as the assimilation of surface pressure data in CERA-20C (Fig. 3 and Table 1). NOAA 20CRv2c and NOAA 20CRv2 display moderate performance in this regard ( $r=0.8$ ,  $RMSE=0.3^{\circ}C$ ) (Fig. 3), and the former reanalysis displays no improvement in performance, despite its use of new boundary conditions (Compo et al., 2011).

### 3.3 Key Factors Regulating Regional Temperature Change

This section discusses key factors that control regional temperature change from the perspective of energy balance and its partitioning. The  $R_s$  heats the surface, and the portion of this radiation that becomes the sensible heat flux heats the air near the

surface (Zhou and Wang, 2016b; Wang and Dickinson, 2013; Zhou and Wang, 2016c). Part of the energy absorbed by the surface is released back to space as outgoing longwave radiation; some of this radiation is reflected by clouds and is influenced by atmospheric water vapor, further warming the near-surface air (Wang and Dickinson, 2013). This process is known as the greenhouse effect on  $T_a$  and is quantified by  $L_d$ . Existing studies have suggested that precipitation frequency better represents the interannual variability in soil moisture in China than the precipitation amount (Wu et al., 2012; Piao et al., 2009; Zhou et al., 2017; Zhou and Wang, 2017a); in turn, soil moisture affects vegetation growth and drives changes in surface characteristics (e.g., surface albedo and roughness). These changes alter the partitioning of available energy and thus regulate changes in  $T_a$ .

Fig. 4 illustrates the partial relationships between the annual anomalies in  $T_a$  and  $R_s$ , the precipitation frequency and  $L_d$ . The results show that  $T_a$  is consistently positively correlated with  $R_s$  (except over the Tibetan Plateau) and  $L_d$ ; however, it is consistently negatively correlated with precipitation frequency in the observations and the twelve reanalysis products (Fig. 4). Based on the observations, the interannual variations in  $T_a$  are jointly determined in part by precipitation frequency and  $L_d$  in Northeast China and the northern part of Northwest China (Fig. 4). All of the reanalyses roughly capture these factors over these regions, although they display differences in the relative magnitudes (Fig. 4). Specifically, ERA-20CM, NOAA 20CRv2c, NOAA 20CRv2 and CFSR exhibit comparable relationships of  $T_a$  with precipitation frequency and  $L_d$ ; however, MERRA, MERRA2, NCEP-R2, ERA-20C,

and CERA-20C overestimate the relationship between  $T_a$  and precipitation frequency, and ERA-Interim, JRA-55, and NCEP-R1 overestimate the relationship of  $T_a$  with  $L_d$  over these regions (Fig. 4).

Over the North China Plain and Middle China, the interannual variations in  $T_a$  are ~~partly jointly~~ determined by  $R_s$ , precipitation frequency and  $L_d$  (Fig. 4). The reanalyses roughly capture the effects of these three factors on  $T_a$ , although they display diverse combinations (Fig. 4). Among these combinations, JRA-55, MERRA2, ERA-20CM and ERA-Interim are comparable to the observations over these regions (Fig. 4). Over Southeast China, the interannual variations in  $T_a$  are primarily regulated by  $L_d$ , precipitation frequency and  $R_s$  (Fig. 4). The reanalyses exhibit slightly overestimated relationships of  $T_a$  with  $R_s$  and underestimated relationships with precipitation frequency (Fig. 4).

Over the Tibetan Plateau, the interannual variations in  $T_a$  are regulated by  $R_s$  and precipitation frequency (Fig. 4). Most of the reanalyses roughly capture the combinations of these factors but exhibit certain differences in the relative effects of  $R_s$  and precipitation frequency on  $T_a$  (Fig. 4). MERRA, MERRA2, NOAA 20CRv2c and NOAA 20CRv2 overestimate the relationships of  $T_a$  with  $R_s$  over the Tibetan Plateau (Fig. 4).

Overall, the spatial patterns of the simulated partial correlation of  $T_a$  with  $R_s$  in the reanalysis products are significantly correlated with those seen in the observations;  $r=0.13-0.35$  ( $p<0.05$ ) for the NWP-like reanalyses, and larger values of  $r=0.24-0.41$  ( $p<0.05$ ) are obtained for the climate reanalyses. Moreover, the spatial patterns in the

sensitivity of  $T_a$  to  $R_s$  exhibit significant correlations ( $r=0.12-0.17$ ,  $p<0.05$ ) for most of the climate reanalyses (Table 1). Precipitation frequency displays the largest spatial correlations ( $r=0.16-0.43$ ,  $p<0.05$ ) of the sensitivity of  $T_a$  with these three relevant parameters in the reanalyses (Table 3). Significant spatial correlations reflecting the relationship (including the partial correlation and sensitivity) of  $T_a$  with  $L_d$  are also found (Table 1).

### 3.4 Regional Warming Trend Biases and Their Causes

#### 1) The Whole of China

From 1979 to 2010 over China,  $T_a$  exhibits strong warming trends of  $0.37^\circ\text{C}/\text{decade}$  ( $p<0.05$ ) in the observations and  $0.22-0.48^\circ\text{C}/\text{decade}$  ( $p<0.05$ ) in the twelve reanalyses (Figs. 5 and S2-S3, Table 2). ERA-Interim and JRA-55 display spatial correlations with the observations ( $r=0.47$  and  $0.54$ ,  $p<0.05$ ) that are due at least partly to the inclusion of some  $T_a$  observations, whereas NCEP-R2 and ERA-20C display the worst performance (Figs. S3, Tables 1 and 3). Furthermore, approximately 87% of the observed trends in  $T_a$  over China can be explained by the greenhouse effect (i.e., 65% can be explained by the trend in  $L_d$ ), precipitation frequency (29%) and  $R_s$  (-7%, due to the trend in radiative forcing of  $-1.1 \text{ W}\cdot\text{m}^{-2}/\text{decade}$ ) (Figs. S3-4). The influence of the greenhouse effect on the observed trends in  $T_a$  consists mainly of the trends in the atmospheric water vapor (42%) and the cloud fraction (3%) (Fig. S5). Among the reanalyses, over 90% of the trend in  $T_a$  can be explained by the greenhouse effect, precipitation frequency and  $R_s$  (Figs. S4-6). Specifically, ERA-Interim, JRA-55, MERRA and MERRA2 display the best ability to

capture the contributions of the greenhouse effect (48% to 76%), precipitation frequency (22% to 34%) and  $R_s$  (-4% to 13%) to the trend in  $T_a$  over China (Figs. S4 and S6). The remaining NWP-like reanalyses (i.e., NCEP-R1 and NCEP-R2) substantially overestimate the contribution of  $R_s$  to the trend in  $T_a$ , whereas the climate reanalyses overestimate the contribution from  $L_d$  (Figs. S4 and S6).

~~Here, w~~We further quantify the contributions to the biases in the trend in  $T_a$  made by those in  $R_s$ ,  $L_d$  and precipitation frequency among the twelve reanalyses over China and its seven subregions (Figs. 6-7). Over China, the overestimated  $R_s$  trends (by 0.00-3.93  $\text{W}\cdot\text{m}^{-2}/\text{decade}$ ; Figs. S8 and S13) increase the trends in  $T_a$  (by 0.02-0.16°C/decade; Fig. 7) in the twelve reanalyses; the underestimated  $L_d$  trends (by -0.25 to -1.61  $\text{W}\cdot\text{m}^{-2}/\text{decade}$  for the NWP-like reanalyses; Figs. S10 and S15) decrease the trends in  $T_a$  (by -0.05 to -0.25°C/decade for the NWP-like reanalyses; Fig. 7); and the biases in the trends in precipitation frequency (by approximately -1.5 days/decade for the NWP-like reanalyses and approximately 2.6 days/decade for the climate reanalyses; Figs. S9 and S14) decrease the trends in  $T_a$  (by 0.01 to 0.05°C/decade for the NWP-like reanalyses and -0.01 to -0.06°C/decade for the climate reanalyses; Fig. 7). Together, these effects produce an underestimate in the trends in  $T_a$  on the order of 0.10°C/decade in the reanalyses (Fig. 7 and Table 2).

## 2) Seven Subregions

~~However, a~~Averaged trends over large areas may mask regional differences that reflect diverse regional warming biases and their causes (Figs. 5-7). The mean-adjusted spatial patterns of the biases in the trends in  $T_a$  appear to be consistent



among the twelve reanalyses (Fig. S7) and mimic the spatial patterns in the overestimated  $R_s$  trends over the North China Plain, South China and Northeast China (Fig. S8), given the spatial correlations between these variables in most of the reanalyses ( $r=0.11-0.42$ ,  $p<0.05$ ) (Figs. 6 and S7-8, Table 3). However, the reanalyses still underestimate the trends in  $T_a$  over most of the regions. The key reason for this underestimation is the increase in precipitation frequency over Northwest China, the Loess Plateau, and Middle China seen in the NWP-like reanalyses and that seen over broader regions in the climate reanalyses (Figs. 5-6 and S9). This relationship is reflected by their negative spatial correlation, which has a maximum value of -0.62 ( $p<0.05$ ) for MERRA (Table 3). Moreover, the decrease in  $L_d$ , which occurs due to the decreases in the atmospheric water vapor and cloud fraction that occur in the NWP-like reanalyses (Figs. S10-12), substantially cancels the warming effect of the overestimation of  $R_s$  on  $T_a$  over eastern China (Figs. 5 and S7). The opposite changes occur over Southeastern China in the climate reanalyses (Figs. 5 and S10). The effect of the changes in  $L_d$  is reflected by its spatial correlations of up to 0.50 ( $p<0.05$ ) (Table 3).

The corresponding contributions to the biases in the  $T_a$  trend from are calculated from those in  $R_s$ ,  $L_d$  and precipitation frequency over seven subregions of China (Figs. 6-7).

~~Here, we further quantify the contributions to the biases in the trend in  $T_a$  made by those in  $R_s$ ,  $L_d$  and precipitation frequency among the twelve reanalyses over China and its seven subregions (Figs. 6-7). Over China, the overestimated  $R_s$  trends (by~~

~~0.00–3.93 W·m<sup>-2</sup>/decade; Figs. S8 and S13) increase the trends in  $T_w$  (by 0.02–0.16°C/decade; Fig. 7) in the twelve reanalyses; the underestimated  $L_d$  trends (by -0.25 to -1.61 W·m<sup>-2</sup>/decade for the NWP-like reanalyses; Figs. S10 and S15) decrease the trends in  $T_w$  (by -0.05 to -0.25°C/decade for the NWP-like reanalyses; Fig. 7); and the biases in the trends in precipitation frequency (by approximately 1.5 days/decade for the NWP-like reanalyses and approximately 2.6 days/decade for the climate reanalyses; Figs. S9 and S14) decrease the trends in  $T_w$  (by 0.01 to 0.05°C/decade for the NWP-like reanalyses and -0.01 to -0.06°C/decade for the climate reanalyses; Fig. 7). Together, these effects produce an underestimate in the trends in  $T_w$  on the order of 0.10°C/decade in the reanalyses (Fig. 7 and Table 2).~~

Over northern China, biases in the trend in  $T_a$  result primarily from those in precipitation frequency and  $L_d$  (Figs. 6-7). Over Northeast China, the observations exhibit an amplified warming of 0.41°C/decade ( $p < 0.05$ ; Fig. 4 and Table 2). This warming is significantly underestimated by NCEP-R1, JRA-55, NOAA 20CRv2 and NOAA 20CRv2c (by on the order of -0.15°C/decade) and is overestimated by MERRA and CFSR (by on the order of 0.2°C/decade) (Figs. 6-7). These biases in the trends in  $T_a$  in the reanalysis are jointly explained by the warming (0.04–0.48°C/decade) induced by the underestimated trends in precipitation frequency and the cooling (-0.04 to -0.42°C/decade) induced by the underestimated trends in  $L_d$  (Fig. 7).

Over Northwest China, the biases in the trend in precipitation frequency and  $L_d$  are mainly explained by the overestimated warming in NCEP-R2 (by 0.22°C/decade)

(Fig. 7). The substantially underestimated trend in  $L_d$  induced by the decrease in the atmospheric water vapour and cloud fraction (Figs. S9-S12 and S16-17) lead to an underestimate of the warming in MERRA (by  $-0.22^{\circ}\text{C}/\text{decade}$ ) (Fig. 7).

Most of the reanalyses display weakened warming over the Tibetan Plateau and the Loess Plateau (Fig. 5 and S3, Table 2). In particular, NCEP-R1 and NCEP-R2 fail to reproduce the warming over the Tibetan Plateau, and MERRA fails to reproduce the warming over the Loess Plateau (Fig. 5 and S3, Table 2). The significant cooling biases in the trends in  $T_a$  (by  $-0.02$  to  $-0.31^{\circ}\text{C}/\text{decade}$ ) over the Tibetan Plateau and the Loess Plateau result from the underestimated trends in  $L_d$  and the overestimated trends in precipitation frequency seen in most of the reanalyses (Figs. 5-7 and S9-12). These cooling biases are further induced by the underestimated trends in  $R_s$  (Figs. 5-7 and S8).

Over southern China, the biases in the trend in  $T_a$  are regulated by the biases in the trends in  $R_s$ ,  $L_d$  and precipitation frequency (Figs. 6-7). Over Southeast China, the significantly overestimated trends in  $T_a$  (by  $0.04$ ,  $0.02$  and  $0.17^{\circ}\text{C}/\text{decade}$ , respectively) are induced by the overestimated trends in  $R_s$  (by  $4.25$ ,  $3.34$  and  $6.27 \text{ W}\cdot\text{m}^{-2}/\text{decade}$ , respectively) seen in ERA-Interim, JRA-55 and CFSR (Figs. 6-7 and S8). The underestimated trends in  $T_a$  are induced by the overestimated trends in precipitation frequency and  $L_d$  in NCEP-R1, MERRA, ERA-20CM, CERA-20C, NOAA 20CRv2 and NOAA 20CRv2c (Figs. 6-7 and S9).

Over Middle China, the significantly overestimated trends in  $T_a$  (by  $0.04$ ,  $0.06$ ,  $0.11$ ,  $0.03$ ,  $0.11$  and  $0.14^{\circ}\text{C}/\text{decade}$ , respectively) are induced by the overestimated

trends in  $R_s$  (by 2.09, 1.50, 2.59, 1.20 and 4.81  $\text{W}\cdot\text{m}^{-2}/\text{decade}$ , respectively) seen in ERA-Interim, JRA-55, ERA-20C, ERA-20CM, CERA-20C and CFSR (Figs. 6-7 and S8). The overestimated trends in precipitation frequency may lead to cooling in the trends in  $T_a$  in the reanalyses, especially for MERRA (which reflects an induced bias in the trend of  $-0.15^\circ\text{C}/\text{decade}$ ) over Middle China (Figs. 6-7 and S9).

Due to the underestimated trends in the atmospheric water vapor and the cloud fraction (Figs. S11-12), the underestimation of  $L_d$  produces a cooling effect on the trend in  $T_a$  (by  $-0.05$  to  $-0.32^\circ\text{C}/\text{decade}$ ) in the reanalyses over the North China Plain (Figs. 6-7 and S10). However, due to the lack of inclusion of plausible trends in aerosol loading, the substantial increases in  $R_s$  over the North China Plain (Fig. S8) have strong warming effects on the trends in  $T_a$  (by  $0.01$  to  $0.21^\circ\text{C}/\text{decade}$ ) in the reanalyses (Figs. 6-7 and S8). The biases in the trends in precipitation frequency (of approximately  $-2.5$  days/decade for the NWP-like reanalyses and approximately  $1.5$  days/decade for some of the climate reanalyses) contribute some part of the biases in the trends in  $T_a$  (approximately  $0.05^\circ\text{C}/\text{decade}$  for the NWP-like reanalyses and  $-0.03^\circ\text{C}/\text{decade}$  for the climate reanalyses).

Overall, the biases in the trends in  $T_a$  in the reanalyses can be substantially explained by those in  $L_d$ , precipitation frequency and  $R_s$ , but this effect varies regionally (Figs. 6-7). Over northern China, the biases in the trend in  $T_a$  (which are on the order of  $-0.12^\circ\text{C}/\text{decade}$ ) result primarily from a combination of those in  $L_d$  (which are on the order of  $-0.10^\circ\text{C}/\text{decade}$ ) and precipitation frequency (which are on the order of  $0.05^\circ\text{C}/\text{decade}$ ), with relatively small contributions from  $R_s$  (which are on

the order of  $-0.03^{\circ}\text{C}/\text{decade}$ ). Over southern China, the biases in the trend in  $T_a$  (which are on the order of  $-0.07^{\circ}\text{C}/\text{decade}$ ) are caused by those in  $R_s$  (which are on the order of  $0.10^{\circ}\text{C}/\text{decade}$ ),  $L_d$  (which are on the order of  $-0.08^{\circ}\text{C}/\text{decade}$ ) and precipitation frequency (which are on the order of  $-0.06^{\circ}\text{C}/\text{decade}$ ) (Fig. S18). ~~Note also that the incorporation of the observed changes in surface air temperatures in ERA-Interim and JRA-55 may introduce biases into the trends in the output  $T_a$  values; however, the use of partial correlation and regression analysis would lead to smaller impacts of the biases in these physical variables in quantifying their contributions to the trends in  $T_a$ .~~

### 3.5 Spatial Linkages of Biases in the Warming Trends in the Twelve Reanalyses

We next integrate the relationships of the spatial patterns in the biases in the trends in  $T_a$  with those in  $R_s$ ,  $L_d$  and precipitation frequency over China in the twelve reanalyses (Fig. 8). The results show that the biases in the trends in  $T_a$  show significant correlations with  $R_s$  ( $r=0.80$ , slope= $0.06$ ,  $p=0.09$ ) and precipitation frequency ( $r=-0.83$ , slope= $-0.04$ ,  $p=0.02$ ) and  $L_d$  ( $r=0.77$ , slope= $0.10$ ,  $p=0.10$ ) in the twelve reanalyses if information on these patterns is included. When the spatial patterns of the biases in the trends in these variables are not considered, the biases in the trends in  $T_a$  show relatively small correlations with  $R_s$  ( $r=0.32$ , slope= $0.02$ ,  $p>0.1$ ), precipitation frequency ( $r=-0.51$ , slope= $-0.02$ ,  $p=0.09$ ) and  $L_d$  ( $r=0.14$ , slope= $0.02$ ,  $p>0.1$ ) in the reanalyses (Fig. 8). Similar results are obtained for the atmospheric water vapor ( $r=0.71$ ,  $p=0.1$ ) and the cloud fraction ( $r=-0.74$ ,  $p=0.09$ ) if their spatial patterns are considered (Figs. S19), and this relationship involving the cloud fraction

is very similar to that associated with  $R_s$  (Figs. 8 and S19). Within the subregions of China, the biases in the trends in  $T_a$  show significant correlations with  $R_s$  ( $r=0.68$  to  $0.90$ ,  $p<0.1$ ), precipitation frequency ( $r=-0.55$  to  $-0.94$ ,  $p<0.1$ ) and  $L_d$  ( $r=0.53$  to  $0.93$ ,  $p<0.1$ ) when the spatial patterns in the reanalyses are included (Fig. S20). These results provide a novel perspective that can be used to investigate the spatial relationships between biases in the trends in  $T_a$  and relevant quantities in reanalyses.

#### 4. Discussion

In this section, we first examine the possible impacts of data homogenization on the trends in  $T_a$ . The trends in  $T_a$  derived from the original dataset are almost as high as those from the homogenized dataset, especially over the North China Plain and Northwest China (Fig. 5 and Table 2). Homogenization primarily adjusts breakpoints in time series (Wang, 2008), which occur mainly due to station relocation and changes in instruments (Cao et al., 2016; Li et al., 2017; Wang, 2014), and it helps to objectively depict trends in  $T_a$ , thus permitting the assessment of the modelled trends in  $T_a$  and its spatial patterns that are present in the reanalyses.

We found that the elevation differences between the models and the stations influence the biases in the trends in  $T_a$  but cannot explain the spatial patterns in the biases in the trends in  $T_a$  (average  $r=0.11$ ) (Fig. S21). Comparison of the models that use the same grid (NOAA 20CRv2c vs. NOAA 20CRv2, MERRA vs. MERRA2, NCEP-R1 vs. NCEP-R2 and ERA-20C vs. ERA-20CM) shows that the one is correlated with elevation differences, but the other is not, which implies that this

statistical correlation does not have physical significance. ~~In addition, elevation differences do not change with time.~~ Nevertheless, the spatial patterns in the normalized trends in  $T_a$  (excluding the impacts of the absolute value of temperature on the trends) are very near to those of the trends (Fig. S22), implying that the differences in the absolute value of temperature have an important effect, given that the site-to-grid inconsistency can be neglected.

In the reanalyses, vegetation is only included as climatological information, but the vegetation displays a growth trend during the study period of 1979-2010 within China (Fig. S23). This discrepancy positively enlarges the biases in the trends in  $T_a$  due to the vegetation cooling effect (Zeng et al., 2017; Trigo et al., 2015). This effect is reflected by the negative spatial correlation ( $r=-0.26$ ,  $p=0.00$ ) between the inverted trend in the NDVI and the biases in the trend in  $T_a$  (Fig. S23). The growth of vegetation reduces  $T_a$  by regulating surface roughness, surface conductivity, soil moisture and albedo to partition greater amounts of available energy into latent heat fluxes, which leads to the formation of more precipitation (Shen et al., 2015; Spracklen et al., 2013). Thus, the inclusion of vegetation growth will improve the simulation of trends and especially the spatial pattern of  $T_a$  in the reanalyses through the incorporation of more complete physical parameterizations (Li et al., 2005; Dee and Todling, 2000; Trigo et al., 2015).

Due to their inclusion of surface air temperature observations, ERA-Interim and JRA-55 display high skill in reproducing the observed patterns; they have near-zero means (0.01 and 0.01°C/decade) and the smallest standard deviations (0.16 and

0.15°C/decade) of the trend biases among the twelve reanalysis products. However, pattern differences of 37.8% (standard deviation of trend bias/China-averaged trend) are still evident (Figs. 5 and 8). Although it does not incorporate surface air temperature observations, ERA-20CM presents a pattern (with a mean of -0.04°C/decade and a standard deviation of 0.15°C/decade; Figs. 5 and 8) that is comparable to those of ERA-Interim and JRA-55 and better than that of ERA-20C (mean of -0.08°C/decade and standard deviation of 0.20°C/decade; Figs. 5 and 8), which uses the same forecast model as ERA-20CM. These results imply that ensemble forecasting could be used to meet important goals. The ensemble [forecastingsimulation](#) technique used in ERA-20CM also displays advantages in that it yields an improved simulated pattern of biases in the trends in  $R_s$  (SD=1.84 W·m<sup>-2</sup>/decade, 171%), precipitation frequency (SD=2.78days/decade, 122%) and  $L_d$  (SD=1.25 W·m<sup>-2</sup>/decade, 82%) (Fig. 8).

We consider the degree to which the ensemble assimilation technique can improve the spatial patterns of the biases in the trends in  $T_a$  in the reanalyses. We find that this technique can detect the biases in the trends in  $T_a$  over more another approximately 12% (8%) of the grid cells in CERA-20C, which incorporates 10 ensemble members (NOAA 20CR2vc and NOAA 20CR2v employ 56 ensemble members) (Figs. 5 l-n). However, the biases in the trends in  $T_a$  over these grid cells are not significant at a significance level of 0.05, according to Student's  $t$ -test, implying that the ensemble assimilation technique cannot explain the spatial pattern of the biases in the trends in  $T_a$  identified in this study (in Figs. 5 l-n).



To provide a preliminary discussion of the improvements in climate forecast models in reflecting patterns in climate trends, we compare the spatial patterns of the biases in the trends in  $R_s$ , precipitation frequency and  $L_d$  ~~in the reanalyses~~ because observations of these variables are that do not incorporate observations included in the reanalyses. We find that the climate forecast models, i.e., ERA-20C, ERA-20CM, CERA-20C, NOAA 20CRv2c and NOAA 20CRv2, display better performance in reproducing the pattern of biases in the trends in  $R_s$  (mean of 1.36 vs. 2.18  $\text{W}\cdot\text{m}^{-2}/\text{decade}$ ; SD of 2.04 vs. 2.71  $\text{W}\cdot\text{m}^{-2}/\text{decade}$ ), precipitation frequency (mean of 1.32 vs. -1.44%/decade; SD of 3.57 vs. 6.14%/decade) and  $L_d$  (mean of 0.12 vs. -0.85  $\text{W}\cdot\text{m}^{-2}/\text{decade}$ ; SD of 1.33 vs. 1.50  $\text{W}\cdot\text{m}^{-2}/\text{decade}$ ) than the NWP-like models, i.e., ERA-Interim, NCEP-R1, MERRA, JRA-55, NCEP-R2 and MERRA2 (Fig. 8). In addition, because the SST boundary condition evolves freely in CFSR, the patterns of biases in the trends in  $R_s$ , precipitation frequency and  $L_d$  in CFSR differ substantially from those in the other reanalyses.

We also consider whether the spatial pattern of biases in the trend in  $T_a$  is altered by the atmospheric circulation patterns simulated by the ERA-20CM ensemble. In ERA-20CM, the atmospheric circulation patterns are influenced by SSTs and sea ice and then partly mediate the influence of global forcings on the trends in  $T_a$ . In ERA-20CM, the probability distribution function of the biases in the trends in  $T_a$  from outside the ensemble ranges incorporates that from Student's  $t$ -test at a significance level of 0.05 (Fig. 5k). This result has important implications in that 1) the climate variability in the ensembles under the different model realizations of SSTs and sea ice

cover does not change the pattern of the biases in the trends in  $T_a$  (Fig. 5k); moreover, 2) Student's  $t$ -test exhibits a suitable ability to detect the significance of the biases in the trends in  $T_a$  (Fig. 5k) when considering the effects of interannual variability on the trend.

Overall, producing global or regional reanalyses that adequately reflect regional climate is challenging using the current strategy, and further improvements are required. The results and discussion above indicate some potential but challenging approaches that can be used to maximize the signal component corresponding to the regional climate in final reanalyses and robustly narrow the uncertainties in trends.

1) MERRA2's pioneering incorporation of time-varying aerosol loadings provides a way of improving the representation of regional temperature changes over regions such as the North China Plain where the impacts of aerosols on surface temperatures are significant~~MERRA2 incorporates time-varying aerosol loadings in a pioneering attempt to improve regional warming over the North China Plain to some extent.~~ Thus, we encourage research groups to include accurate aerosol information and improve the skill of simulation of the energy budget and partitioning, especially of regional surface incident solar radiation, in other reanalyses.

2) To improve regional climate modelling, forecast output should be produced using a physical ensemble like that employed in ERA-20CM to quantify the uncertainties associated with the relevant parameterizations in the reanalyses, due to the impossibility of optimizing all of the biases. Meanwhile, careful ensemble design would likely yield useful information for use in improving models, assimilation

730 methods and the bias correction of observations by exploring the interdependency  
731 among sources of errors. Such designs would undoubtedly have additional benefits for  
732 further development, leading to the next generation of reanalyses.

733 3) To improve coupled land-atmospheric interactions, the true dynamics of land  
734 cover and use should be incorporated. Moreover, the physical parameterizations  
735 should be improved, including the responses of surface roughness, surface  
736 conductivity and albedo to regional climate. These changes would represent an  
737 improvement over the use of constant types and fractions of vegetation, as is done in  
738 ERA-Interim (Zhou and Wang, 2016b).

739 4) Given the implications of the spurious performance of the freely evolving  
740 boundary conditions in CFSR, homogeneous and accurate records of SST and sea ice  
741 should be produced.

742 Next-generation reanalyses, including both global and regional reanalyses, will  
743 assimilate and analyse *in situ* observations, satellite radiance, and other remote  
744 observations. In addition to short-term accuracy and long-term trends, they will also  
745 focus on spatial patterns by incorporating or improving accurate representations of  
746 land surface conditions and processes within the coupled weather and climate Earth  
747 systems. Thus, these reanalyses will advance the simulation of land-atmosphere  
748 interactions to yield high skill in studies of regional warming and the detection and  
749 attribution of regional climate change using various datasets, which frequently include  
750 global and regional reanalyses (Zhou et al., 2018; Zhou and Wang, 2016d; Herring et  
751 al., 2018; Trenberth et al., 2015; Stott, 2016; Dai et al., 2017; Zhou and Wang, 2017b).

752 Additionally, the uncertainties associated with regional warming could be ascertained  
753 using physics ensembles with various equiprobable realizations of boundary  
754 conditions.

## 756 5. Conclusions

757 The reanalyses display differences in  $T_a$  when compared to the observations with  
758 a range of  $-10\sim 10^\circ\text{C}$  over China. Approximately 74% and 6% of these differences can  
759 be explained by site-to-grid elevation differences and the filtering error in the  
760 elevations used in the spectral models. These results imply fairly good skill in the  
761 simulation of the climatology of  $T_a$  in the twelve reanalyses over China. Moreover,  
762 the twelve reanalyses roughly capture the interannual variability in  $T_a$  (median  
763  $r=0.95$ ). In the reanalyses,  $T_a$  displays a consistently positive correlation with  $R_s$  and  
764  $L_d$  and is negatively correlated with precipitation frequency, as seen in observations,  
765 despite the evident spatial patterns in their magnitudes over China.

766  $T_a$  exhibits a strong warming trend of  $0.37^\circ\text{C}/\text{decade}$  ( $p<0.05$ ) in the observations  
767 and  $0.22\text{-}0.48^\circ\text{C}/\text{decade}$  ( $p<0.05$ ) in the twelve reanalyses over China. In the  
768 observations, approximately 87% of the observed trend in  $T_a$  over China can be  
769 explained by the greenhouse effect (i.e., 65% can be explained by the trend in  $L_d$ ),  
770 precipitation frequency (29%) and  $R_s$  (-7%, due to the trend in radiative forcing of  
771  $-1.1\text{ W}\cdot\text{m}^{-2}/\text{decade}$ ).

772 However, the biases in the trends in  $T_a$  seen in the reanalyses relative to the  
773 observations display an evident spatial pattern (mean= $-0.16\sim 0.11^\circ\text{C}/\text{decade}$ ,

SD=0.15-0.30°C/decade). The spatial patterns of the biases in the trends in the values of  $T_a$  in the reanalyses are significantly correlated with those in  $R_s$  (maximum  $r=0.42$ ,  $p<0.05$ ), precipitation frequency (maximum  $r=-0.62$ ,  $p<0.05$ ) and  $L_d$  (maximum  $r=0.50$ ,  $p<0.05$ ). Over northern China, the biases in the trends in  $T_a$  (which are on the order of -0.12°C/decade) result primarily from a combination of those in  $L_d$  (which are on the order of -0.10°C/decade) and precipitation frequency (which are on the order of 0.05°C/decade), with relatively small contributions from  $R_s$  (which are on the order of -0.03°C/decade). Over southern China, the biases in the trends in  $T_a$  (which are on the order of -0.07°C/decade) are regulated by the biases in the trends in  $R_s$  (which are on the order of 0.10°C/decade),  $L_d$  (which are on the order of -0.08°C/decade) and precipitation frequency (which are on the order of -0.06°C/decade).

If information on spatial patterns is included, the simulated biases in the trends in  $T_a$  correlate well with those of precipitation frequency,  $R_s$  and  $L_d$  in the reanalyses ( $r=-0.83$ ,  $0.80$  and  $0.77$ ,  $p<0.1$ ); similar results are obtained for the atmospheric water vapor and the cloud fraction ( $r=0.71$  and  $-0.74$ ,  $p<0.1$ ). These results provide a novel perspective that can be used to investigate the spatial relationships between the biases in the trends in  $T_a$  and the relevant parameters among the twelve reanalyses. Therefore, improving simulations of precipitation frequency and  $R_s$  helps to maximize the signal component corresponding to the regional climate. In addition, [the analysis of  \$T\_a\$  observations helps to improve the performance of regional warming in ERA-Interim and JRA-55.](#) Incorporating vegetation dynamics in reanalyses and the use of accurate

aerosol information, as in MERRA-2, would advance the modelling of regional warming. The ensemble technique adopted in ERA-20CM, a twentieth-century atmospheric model ensemble that does not assimilate observations, significantly narrows the uncertainties of regional warming in the reanalyses (standard deviation=0.15°C/decade).

**Acknowledgements** This study was funded by the National Key R&D Program of China (2017YFA0603601) and the National Natural Science Foundation of China (41525018). The latest observational datasets were obtained from the China Meteorological Administration (CMA; <http://www.cma.gov.cn>). Considerable gratitude is owed to several reanalysis working teams, including the European Centre for Medium-Range Weather Forecasts (ECMWF) for providing the ERA-Interim, ERA-20C, ERA-20CM and CERA-20C data (<http://www.ecmwf.int/>); the Global Modelling and Assimilation Office (GMAO) at the NASA Goddard Space Flight Center for providing the MERRA and MERRA2 data (<http://gmao.gsfc.nasa.gov/>); the NOAA Earth System Research Laboratory (ESRL) for providing the NCEP-R1, NCEP-R2, CFSR, NOAA 20CRv2 and NOAA 20CRv2c data (<http://www.esrl.noaa.gov/>); and the Climate Prediction Division of the Global Environment and Marine Department at the Japan Meteorological Agency for providing the JRA-55 data (<http://jra.kishou.go.jp/>). We thank the Expert Team on Climate Change Detection and Indices (ETCCDI) for providing the RHtestV4 package (<http://etccdi.pacificclimate.org/software.shtml>), the United States

818 Geological Survey Earth Resources Observation and Science Data Center for  
819 providing the GTOPO30 data  
820 (<http://edc.usgs.gov/products/elevation/gtopo30/gtopo30.html>) and the working team  
821 of the Global Inventory Monitoring and Modelling System (GIMMS) project  
822 (<https://ecocast.arc.nasa.gov/data/pub/gimms/>). We thank Kevin E. Trenberth for his  
823 insightful suggestions.

## References

- Aarnes, O. J., Abdalla, S., Bidlot, J.-R., and Breivik, Ø.: Marine wind and wave height trends at different ERA-Interim forecast ranges, *J. Clim.*, 28, 819-837, 10.1175/jcli-d-14-00470.1, 2015.
- Andersson, E., Bauer, P., Beljaars, A., Chevallier, F., Holm, E., Janiskova, M., Kallberg, P., Kelly, G., Lopez, P., McNally, A., Moreau, E., Simmons, A. J., Thepaut, J. N., and Tompkins, A. M.: Assimilation and modeling of the atmospheric hydrological cycle in the ECMWF forecasting system, *Bull. Am. Meteorol. Soc.*, 86, 387-402, 10.1175/bams-86-3-387, 2005.
- Balsamo, G., Albergel, C., Beljaars, A., Boussetta, S., Brun, E., Cloke, H., Dee, D., Dutra, E., Muñoz-Sabater, J., Pappenberger, F., de Rosnay, P., Stockdale, T., and Vitart, F.: ERA-Interim/Land: a global land surface reanalysis data set, *Hydrol. Earth Syst. Sci.*, 19, 389-407, 10.5194/hess-19-389-2015, 2015.
- Bauer, P., Thorpe, A., and Brunet, G.: The quiet revolution of numerical weather prediction, *Nature*, 525, 47-55, 10.1038/nature14956, 2015.
- Bengtsson, L., Kanamitsu, M., Kallberg, P., and Uppala, S.: FGGE research activities at ECMWF, *Bull. Am. Meteorol. Soc.*, 63, 227-303, 1982a.
- Bengtsson, L., Kanamitsu, M., Kallberg, P., and Uppala, S.: FGGE 4-dimensional data assimilation at ECMWF, *Bull. Am. Meteorol. Soc.*, 63, 29-43, 1982b.
- Bengtsson, L., and Shukla, J.: Integration of space and in situ observations to study global climate change, *Bull. Am. Meteorol. Soc.*, 69, 1130-1143, 10.1175/1520-0477(1988)069<1130:iosais>2.0.co;2, 1988.
- Bengtsson, L., Hagemann, S., and Hodges, K. I.: Can climate trends be calculated from reanalysis data?, *J Geophys Res-Atmos*, 109, D11111, 10.1029/2004jd004536, 2004.
- Bengtsson, L., Haines, K., Hodges, K. I., Arkin, P., Berrisford, P., Bougeault, P., Kallberg, P., Simmons, A. J., Uppala, S., Folland, C. K., Gordon, C., Rayner, N., Thorne, P. W., Jones, P., Stammer, D., and Vose, R. S.: The need for a dynamical climate reanalysis, *Bull. Am. Meteorol. Soc.*, 88, 495-501, 10.1175/bams-88-4-495, 2007.
- Betts, A. K., Hong, S.-Y., and Pan, H.-L.: Comparison of NCEP-NCAR reanalysis with 1987 FIFE data, *Monthly Weather Review*, 124, 1480-1498, 10.1175/1520-0493(1996)124<1480:connrw>2.0.co;2, 1996.
- Betts, A. K., Viterbo, P., and Beljaars, A. C. M.: Comparison of the land-surface interaction in the ECMWF reanalysis model with the 1987 FIFE data, *Monthly Weather Review*, 126, 186-198, 10.1175/1520-0493(1998)126<0186:cotlsi>2.0.co;2,



1998.

Betts, A. K.: Understanding hydrometeorology using global models, *Bull. Am. Meteorol. Soc.*, 85, 1673-1688, 10.1175/bams-85-11-1673, 2004.

Bilbao, J., and De Miguel, A. H.: Estimation of daylight downward longwave atmospheric irradiance under clear-sky and all-sky conditions, *J. Appl. Meteor. Climatol.*, 46, 878-889, 2007.

Brunt, D.: Notes on radiation in the atmosphere. I, *Q. J. Roy. Meteorol. Soc.*, 58, 389-420, 1932.

Cao, L., Zhu, Y., Tang, G., Yuan, F., and Yan, Z.: Climatic warming in China according to a homogenized data set from 2419 stations, *Int. J. Climatol.*, 36, 4384-4392, 10.1002/joc.4639, 2016.

Cash, B. A., III, J. L. K., Adams, J., Altshuler, E., Huang, B., Jin, E. K., Manganello, J., Marx, L., and Jung, T.: Regional structure of the Indian summer monsoon in observations, reanalysis, and simulation, *J. Clim.*, 28, 1824-1841, 10.1175/jcli-d-14-00292.1, 2015.

Chen, J., Del Genio, A. D., Carlson, B. E., and Bosilovich, M. G.: The spatiotemporal structure of twentieth-century climate variations in observations and reanalyses. Part I: Long-term trend, *J. Clim.*, 21, 2611-2633, 2008.

Choi, M., Jacobs, J. M., and Kustas, W. P.: Assessment of clear and cloudy sky parameterizations for daily downwelling longwave radiation over different land surfaces in Florida, USA, *Geophys. Res. Lett.*, 35, L20402, 2008.

Compo, G. P., Whitaker, J. S., Sardeshmukh, P. D., Matsui, N., Allan, R. J., Yin, X., Gleason, B. E., Vose, R. S., Rutledge, G., Bessemoulin, P., Brönnimann, S., Brunet, M., Crouthamel, R. I., Grant, A. N., Groisman, P. Y., Jones, P. D., Kruk, M. C., Kruger, A. C., Marshall, G. J., Maugeri, M., Mok, H. Y., Nordli, Ø., Ross, T. F., Trigo, R. M., Wang, X. L., Woodruff, S. D., and Worley, S. J.: The twentieth century reanalysis project, *Q. J. Roy. Meteorol. Soc.*, 137, 1-28, 10.1002/qj.776, 2011.

Compo, G. P., Sardeshmukh, P. D., Whitaker, J. S., Brohan, P., Jones, P. D., and McColl, C.: Independent confirmation of global land warming without the use of station temperatures, *Geophys. Res. Lett.*, 40, 3170-3174, 2013.

Cornes, R. C., and Jones, P. D.: How well does the ERA-Interim reanalysis replicate trends in extremes of surface temperature across Europe?, *J Geophys Res-Atmos*, 118, 10262-10276, 10.1002/jgrd.50799, 2013.

Dai, A., Wang, J., Thorne, P. W., Parker, D. E., Haimberger, L., and Wang, X. L.: A new approach to homogenize daily radiosonde humidity data, *J. Clim.*, 24, 965-991, 10.1175/2010jcli3816.1, 2011.

896 Dai, A., Rasmussen, R. M., Liu, C., Ikeda, K., and Prein, A. F.: A new mechanism for  
 897 warm-season precipitation response to global warming based on  
 898 convection-permitting simulations, *Clim. Dyn.*, published online,  
 899 10.1007/s00382-017-3787-6, 2017.

900 Dee, D. P., and Da Silva, A. M.: Data assimilation in the presence of forecast bias, *Q.*  
 901 *J. Roy. Meteorol. Soc.*, 124, 269-295, 1998.

902 Dee, D. P., and Todling, R.: Data assimilation in the presence of forecast bias: The  
 903 GEOS moisture analysis, *Monthly Weather Review*, 128, 3268-3282,  
 904 10.1175/1520-0493(2000)128<3268:daitpo>2.0.co;2, 2000.

905 Dee, D. P.: Bias and data assimilation, *Q. J. Roy. Meteorol. Soc.*, 131, 3323-3343,  
 906 2005.

907 Dee, D. P., and Uppala, S.: Variational bias correction of satellite radiance data in the  
 908 ERA-Interim reanalysis, *Q. J. Roy. Meteorol. Soc.*, 135, 1830-1841, 10.1002/qj.493,  
 909 2009.

910 Dee, D. P., Källén, E., Simmons, A. J., and Haimberger, L.: Comments on  
 911 “Reanalyses suitable for characterizing long-term trends”, *Bull. Am. Meteorol. Soc.*,  
 912 92, 65-70, 10.1175/2010BAMS3070.1, 2011a.

913 Dee, D. P., Uppala, S. M., Simmons, A. J., Berrisford, P., Poli, P., Kobayashi, S.,  
 914 Andrae, U., Balmaseda, M. A., Balsamo, G., Bauer, P., Bechtold, P., Beljaars, A. C.  
 915 M., van de Berg, L., Bidlot, J., Bormann, N., Delsol, C., Dragani, R., Fuentes, M.,  
 916 Geer, A. J., Haimberger, L., Healy, S. B., Hersbach, H., Hólm, E. V., Isaksen, L.,  
 917 Kållberg, P., Köhler, M., Matricardi, M., McNally, A. P., Monge-Sanz, B. M.,  
 918 Morcrette, J. J., Park, B. K., Peubey, C., de Rosnay, P., Tavolato, C., Thépaut, J. N.,  
 919 and Vitart, F.: The ERA-Interim reanalysis: configuration and performance of the data  
 920 assimilation system, *Q. J. Roy. Meteorol. Soc.*, 137, 553-597, 10.1002/qj.828, 2011b.

921 Dee, D. P., Balmaseda, M., Balsamo, G., Engelen, R., Simmons, A. J., and Thépaut, J.  
 922 N.: Toward a consistent reanalysis of the climate system, *Bull. Am. Meteorol. Soc.*, 95,  
 923 1235-1248, 10.1175/bams-d-13-00043.1, 2014.

924 Desroziers, G., Berre, L., Chapnik, B., and Poli, P.: Diagnosis of observation,  
 925 background and analysis - error statistics in observation space, *Q. J. Roy. Meteorol.*  
 926 *Soc.*, 131, 3385-3396, 2005.

927 Dolinar, E. K., Dong, X., and Xi, B.: Evaluation and intercomparison of clouds,  
 928 precipitation, and radiation budgets in recent reanalyses using satellite-surface  
 929 observations, *Clim. Dyn.*, 46, 2123-2144, 10.1007/s00382-015-2693-z, 2016.

930 Fang, J.-Y., and Yoda, K.: Climate and vegetation in China (I). Changes in the  
 931 altitudinal lapse rate of temperature and distribution of sea level temperature, *Ecol.*  
 932 *Res.*, 3, 37-51, 1988.

933 Fujiwara, M., Wright, J. S., Manney, G. L., Gray, L. J., Anstey, J., Birner, T., Davis, S.,  
 934 Gerber, E. P., Harvey, V. L., Hegglin, M. I., Homeyer, C. R., Knox, J. A., Kruger, K.,  
 935 Lambert, A., Long, C. S., Martineau, P., Molod, A., Monge-Sanz, B. M., Santee, M.  
 936 L., Tegtmeier, S., Chabrillat, S., Tan, D. G. H., Jackson, D. R., Polavarapu, S., Compo,  
 937 G. P., Dragani, R., Ebisuzaki, W., Harada, Y., Kobayashi, C., McCarty, W., Onogi, K.,  
 938 Pawson, S., Simmons, A., Wargan, K., Whitaker, J. S., and Zou, C.-Z.: Introduction to  
 939 the SPARC reanalysis intercomparison project (S-RIP) and overview of the reanalysis  
 940 systems, *Atmos. Chem. Phys.*, 17, 1417-1452, 10.5194/acp-17-1417-2017, 2017.

941 Gervais, M., Gyakum, J. R., Atallah, E., Tremblay, L. B., and Neale, R. B.: How well  
 942 are the distribution and extreme values of daily precipitation over North America  
 943 represented in the community climate system model? A comparison to reanalysis,  
 944 satellite, and gridded station data, *J. Clim.*, 27, 5219-5239, 10.1175/jcli-d-13-00320.1,  
 945 2014.

946 Gibson, J., Kallberg, P., Uppala, S., Nomura, A., Hernandez, A., and Simmons, S.: ERA  
 947 description, ECMWF. ERA-15 Project Report Series 1, European Centre for  
 948 Medium-range Weather Forecasts, Reading, UK., 1997.

949 Golub, G. H., and Van Loan, C. F.: An analysis of the total least squares problem,  
 950 *SIAM J. Numer. Anal.*, 17, 883-893, 1980.

951 Heng, Z., Fu, Y., Liu, G., Zhou, R., Wang, Y., Yuan, R., Guo, J., and Dong, X.: A  
 952 study of the distribution and variability of cloud water using ISCCP, SSM/I cloud  
 953 product, and reanalysis datasets, *J. Clim.*, 27, 3114-3128, 10.1175/jcli-d-13-00031.1,  
 954 2014.

955 Herring, S. C., Christidis, N., Hoell, A., Kossin, J. P., Schreck III, C., and Stott, P. A.:  
 956 Explaining extreme events of 2016 from a climate perspective, *Bull. Am. Meteorol.*  
 957 *Soc.*, 99, S1-S157, 2018.

958 Hersbach, H., Peubey, C., Simmons, A., Berrisford, P., Poli, P., and Dee, D.:  
 959 ERA-20CM: a twentieth-century atmospheric model ensemble, *Q. J. Roy. Meteorol.*  
 960 *Soc.*, 141, 2350-2375, 10.1002/qj.2528, 2015.

961 Hines, K. M., Bromwich, D. H., and Marshall, G. J.: Artificial surface pressure trends  
 962 in the NCEP-NCAR reanalysis over the southern ocean and Antarctica, *J. Clim.*, 13,  
 963 3940-3952, 10.1175/1520-0442(2000)013<3940:asptit>2.0.co;2, 2000.

964 Hyk, W., and Stojek, Z.: Quantifying uncertainty of determination by standard  
 965 additions and serial dilutions methods taking into account standard uncertainties in  
 966 both axes, *Anal. Chem.*, 85, 5933-5939, 2013.

967 Kalnay, E., Kanamitsu, M., Kistler, R., Collins, W., Deaven, D., Gandin, L., Iredell,  
 968 M., Saha, S., White, G., and Woollen, J.: The NCEP/NCAR 40-year reanalysis project,  
 969 *Bull. Am. Meteorol. Soc.*, 77, 437-471, 1996.

970 Kanamitsu, M., Ebisuzaki, W., Woollen, J., Yang, S.-K., Hnilo, J. J., Fiorino, M., and  
971 Potter, G. L.: NCEP–DOE AMIP-II Reanalysis (R-2), *Bull. Am. Meteorol. Soc.*, 83,  
972 1631-1643, 10.1175/BAMS-83-11-1631, 2002.

973 Kidston, J., Frierson, D. M. W., Renwick, J. A., and Vallis, G. K.: Observations,  
974 simulations, and dynamics of jet stream variability and annular modes, *J. Clim.*, 23,  
975 6186-6199, 10.1175/2010jcli3235.1, 2010.

976 Kobayashi, S., Ota, Y., Harada, Y., Ebata, A., Moriya, M., Onoda, H., Onogi, K.,  
977 Kamahori, H., Kobayashi, C., Endo, H., Miyaoka, K., and Takahashi, K.: The JRA-55  
978 reanalysis: general specifications and basic characteristics, *J. Meteorol. Soc. Jpn.*, 93,  
979 5-48, 10.2151/jmsj.2015-001, 2015.

980 Lahoz, W. A., and Schneider, P.: Data assimilation: making sense of Earth  
981 Observation, *Front. Environ. Sci.*, 2, 1-28, 10.3389/fenvs.2014.00016, 2014.

982 Laloyaux, P., Balmaseda, M., Dee, D., Mogensen, K., and Janssen, P.: A coupled data  
983 assimilation system for climate reanalysis, *Q. J. Roy. Meteorol. Soc.*, 142, 65-78,  
984 10.1002/qj.2629, 2016.

985 Li, H. B., Robock, A., Liu, S. X., Mo, X. G., and Viterbo, P.: Evaluation of reanalysis  
986 soil moisture simulations using updated Chinese soil moisture observations, *J.*  
987 *Hydrometeorol.*, 6, 180-193, 10.1175/jhm416.1, 2005.

988 Li, Q., Zhang, L., Xu, W., Zhou, T., Wang, J., Zhai, P., and Jones, P.: Comparisons of  
989 Time Series of Annual Mean Surface Air Temperature for China since the 1900s:  
990 Observations, Model Simulations, and Extended Reanalysis, *Bull. Am. Meteorol. Soc.*,  
991 98, 699-711, 10.1175/bams-d-16-0092.1, 2017.

992 Li, Y., Zeng, Z. Z., Zhao, L., and Piao, S. L.: Spatial patterns of climatological  
993 temperature lapse rate in mainland China: A multi-time scale investigation, *J Geophys*  
994 *Res-Atmos*, 120, 2661-2675, Doi 10.1002/2014jd022978, 2015.

995 Lin, R., Zhou, T., and Qian, Y.: Evaluation of global monsoon precipitation changes  
996 based on five reanalysis datasets, *J. Clim.*, 27, 1271-1289,  
997 doi:10.1175/JCLI-D-13-00215.1, 2014.

998 Lindsay, R., Wensnahan, M., Schweiger, A., and Zhang, J.: Evaluation of seven  
999 different atmospheric reanalysis products in the Arctic, *J. Clim.*, 27, 2588-2606,  
1000 10.1175/jcli-d-13-00014.1, 2014.

1001 Ma, L., Zhang, T., Li, Q., Frauenfeld, O. W., and Qin, D.: Evaluation of ERA-40,  
1002 NCEP-1, and NCEP-2 reanalysis air temperatures with ground-based measurements  
1003 in China, *J. Geophys. Res. D Atmos.*, 113, D15115, 10.1029/2007JD009549, 2008.

1004 Mao, J., Shi, X., Ma, L., Kaiser, D. P., Li, Q., and Thornton, P. E.: Assessment of  
1005 reanalysis daily extreme temperatures with china's homogenized historical dataset

1006 during 1979-2001 using probability density functions, *J. Clim.*, 23, 6605-6623,  
1007 10.1175/2010jcli3581.1, 2010.

1008 Mitas, C. M., and Clement, A.: Recent behavior of the Hadley cell and tropical  
1009 thermodynamics in climate models and reanalyses, *Geophys. Res. Lett.*, 33, L01810,  
1010 10.1029/2005gl024406, 2006.

1011 Nguyen, H., Evans, A., Lucas, C., Smith, I., and Timbal, B.: The Hadley circulation in  
1012 reanalyses: climatology, variability, and change, *J. Clim.*, 26, 3357-3376,  
1013 10.1175/jcli-d-12-00224.1, 2013.

1014 Niznik, M. J., and Lintner, B. R.: Circulation, moisture, and precipitation relationships  
1015 along the south Pacific convergence zone in reanalyses and CMIP5 models, *J. Clim.*,  
1016 26, 10174-10192, 10.1175/jcli-d-13-00263.1, 2013.

1017 Onogi, K., Tsltsui, J., Koide, H., Sakamoto, M., Kobayashi, S., Hatsushika, H.,  
1018 Matsumoto, T., Yamazaki, N., Kaalhor, H., Takahashi, K., Kadokura, S., Wada, K.,  
1019 Kato, K., Oyama, R., Ose, T., Mannoji, N., and Taira, R.: The JRA-25 reanalysis, *J.*  
1020 *Meteorol. Soc. Jpn.*, 85, 369-432, Doi 10.2151/Jmsj.85.369, 2007.

1021 Parker, W. S.: Reanalyses and observations: What's the difference?, *Bull. Am.*  
1022 *Meteorol. Soc.*, 97, 1565-1572, 10.1175/bams-d-14-00226.1, 2016.

1023 Peña, M., and Toth, Z.: Estimation of analysis and forecast error variances, *Tellus A*,  
1024 66, 21767, 2014.

1025 Piao, S. L., Yin, L., Wang, X. H., Ciais, P., Peng, S. S., Shen, Z. H., and Seneviratne,  
1026 S. I.: Summer soil moisture regulated by precipitation frequency in China, *Environ.*  
1027 *Res. Lett.*, 4, 044012, 10.1088/1748-9326/4/4/044012, 2009.

1028 Pitman, A. J., and Perkins, S. E.: Global and regional comparison of daily 2-m and  
1029 1000-hpa maximum and minimum temperatures in three global reanalyses, *J. Clim.*,  
1030 22, 4667-4681, 10.1175/2009jcli2799.1, 2009.

1031 Poli, P., Hersbach, H., Dee, D. P., Berrisford, P., Simmons, A. J., Vitart, F., Laloyaux,  
1032 P., Tan, D. G. H., Peubey, C., Thépaut, J.-N., Trémolet, Y., Hólm, E. V., Bonavita, M.,  
1033 Isaksen, L., and Fisher, M.: ERA-20C: An atmospheric reanalysis of the twentieth  
1034 century, *J. Clim.*, 29, 4083-4097, 10.1175/JCLI-D-15-0556.1, 2016.

1035 Reed, B. C.: Linear least - squares fits with errors in both coordinates, *Am. J. Phys.*,  
1036 57, 642-646, 1989.

1037 Reichle, R. H., Koster, R. D., De Lannoy, G. J. M., Forman, B. A., Liu, Q.,  
1038 Mahanama, S. P. P., and Touré, A.: Assessment and enhancement of MERRA land  
1039 surface hydrology estimates, *J. Clim.*, 24, 6322-6338, 10.1175/JCLI-D-10-05033.1,  
1040 2011.

1041 Reichle, R. H., Liu, Q., Koster, R. D., Draper, C. S., Mahanama, S. P. P., and Partyka,  
1042 G. S.: Land surface precipitation in MERRA-2, *J. Clim.*, 30, 1643-1664,  
1043 10.1175/jcli-d-16-0570.1, 2017.

1044 Reuten, C., Moore, R. D., and Clarke, G. K. C.: Quantifying differences between 2-m  
1045 temperature observations and reanalysis pressure-level temperatures in northwestern  
1046 North America, *J. Appl. Meteor. Climatol.*, 50, 916-929, 10.1175/2010jamc2498.1,  
1047 2011.

1048 Rienecker, M. M., Suarez, M. J., Gelaro, R., Todling, R., Bacmeister, J., Liu, E.,  
1049 Bosilovich, M. G., Schubert, S. D., Takacs, L., Kim, G.-K., Bloom, S., Chen, J.,  
1050 Collins, D., Conaty, A., da Silva, A., Gu, W., Joiner, J., Koster, R. D., Lucchesi, R.,  
1051 Molod, A., Owens, T., Pawson, S., Pegion, P., Redder, C. R., Reichle, R., Robertson, F.  
1052 R., Ruddick, A. G., Sienkiewicz, M., and Woollen, J.: MERRA: NASA's Modern-Era  
1053 Retrospective Analysis for Research and Applications, *J. Clim.*, 24, 3624-3648,  
1054 10.1175/JCLI-D-11-00015.1, 2011.

1055 Ryan, T. P.: Modern regression methods, John Wiley & Sons, 2008.

1056 Saha, S., Moorthi, S., Pan, H. L., Wu, X. R., Wang, J. D., Nadiga, S., Tripp, P., Kistler,  
1057 R., Woollen, J., Behringer, D., Liu, H. X., Stokes, D., Grumbine, R., Gayno, G., Wang,  
1058 J., Hou, Y. T., Chuang, H. Y., Juang, H. M. H., Sela, J., Iredell, M., Treadon, R., Kleist,  
1059 D., Van Delst, P., Keyser, D., Derber, J., Ek, M., Meng, J., Wei, H. L., Yang, R. Q.,  
1060 Lord, S., Van den Dool, H., Kumar, A., Wang, W. Q., Long, C., Chelliah, M., Xue, Y.,  
1061 Huang, B. Y., Schemm, J. K., Ebisuzaki, W., Lin, R., Xie, P. P., Chen, M. Y., Zhou, S.  
1062 T., Higgins, W., Zou, C. Z., Liu, Q. H., Chen, Y., Han, Y., Cucurull, L., Reynolds, R.  
1063 W., Rutledge, G., and Goldberg, M.: The NCEP climate forecast system reanalysis,  
1064 *Bull. Am. Meteorol. Soc.*, 91, 1015-1057, 10.1175/2010BAMS3001.1, 2010.

1065 Schoeberl, M. R., Dessler, A. E., and Wang, T.: Simulation of stratospheric water  
1066 vapor and trends using three reanalyses, *Atmos. Chem. Phys.*, 12, 6475-6487,  
1067 10.5194/acp-12-6475-2012, 2012.

1068 Shen, M., Piao, S., Jeong, S.-J., Zhou, L., Zeng, Z., Ciais, P., Chen, D., Huang, M., Jin,  
1069 C.-S., and Li, L. Z.: Evaporative cooling over the Tibetan Plateau induced by  
1070 vegetation growth, *Proc. Nat. Acad. Sci. U.S.A.*, 112, 9299-9304, 2015.

1071 Simmonds, I., and Keay, K.: Mean Southern Hemisphere extratropical cyclone  
1072 behavior in the 40-year NCEP-NCAR reanalysis, *J. Clim.*, 13, 873-885,  
1073 10.1175/1520-0442(2000)013<0873:mshecb>2.0.co;2, 2000.

1074 Simmons, A. J., Willett, K. M., Jones, P. D., Thorne, P. W., and Dee, D. P.:  
1075 Low-frequency variations in surface atmospheric humidity, temperature, and  
1076 precipitation: Inferences from reanalyses and monthly gridded observational data sets,  
1077 *J. Geophys. Res. D Atmos.*, 115, D01110, 10.1029/2009JD012442, 2010.

- 1078 Siswanto, S., Oldenborgh, G. J., Schrier, G., Jilderda, R., and Hurk, B.: Temperature,  
1079 extreme precipitation, and diurnal rainfall changes in the urbanized Jakarta city during  
1080 the past 130 years, *Int. J. Climatol.*, 36, 3207-3225, 2015.
- 1081 Spracklen, D. V., Arnold, S. R., and Taylor, C. M.: Observations of increased tropical  
1082 rainfall preceded by air passage over forests, *Nature*, 494, 390-390,  
1083 10.1038/nature11904, 2013.
- 1084 Stott, P.: How climate change affects extreme weather events, *Science*, 352,  
1085 1517-1518, 10.1126/science.aaf7271, 2016.
- 1086 Tang, W.-J., Yang, K., Qin, J., Cheng, C., and He, J.: Solar radiation trend across  
1087 China in recent decades: a revisit with quality-controlled data, *Atmos. Chem. Phys.*,  
1088 11, 393-406, 2011.
- 1089 Tellinghuisen, J.: Least-squares analysis of data with uncertainty in x and y: A Monte  
1090 Carlo methods comparison, *Chemom. Intell. Lab. Syst.*, 103, 160-169, 2010.
- 1091 Thorne, P., and Vose, R.: Reanalyses suitable for characterizing long-term trends: Are  
1092 they really achievable?, *Bull. Am. Meteorol. Soc.*, 91, 353-361, 2010.
- 1093 Trenberth, K. E., and Olson, J. G.: An evaluation and intercomparison of global  
1094 analyses from the National-Meteorological-Center and the  
1095 European-Centre-for-Medium-Range-Weather-Forecasts, *Bull. Am. Meteorol. Soc.*,  
1096 69, 1047-1057, Doi 10.1175/1520-0477(1988)069<1047:Aeaio>2.0.Co;2, 1988.
- 1097 Trenberth, K. E., Koike, T., and Onogi, K.: Progress and prospects for reanalysis for  
1098 weather and climate, *Eos Trans. Am. Geophys. Union*, 89, 234-235,  
1099 10.1029/2008EO260002, 2008.
- 1100 Trenberth, K. E., Fasullo, J. T., and Shepherd, T. G.: Attribution of climate extreme  
1101 events, *Nature Clim. Change*, 5, 725-730, 10.1038/nclimate2657, 2015.
- 1102 Trigo, I., Boussetta, S., Viterbo, P., Balsamo, G., Beljaars, A., and Sandu, I.:  
1103 Comparison of model land skin temperature with remotely sensed estimates and  
1104 assessment of surface - atmosphere coupling, *J. Geophys. Res. D Atmos.*, 120,  
1105 D023812, 10.1002/2015JD023812, 2015.
- 1106 Tsidu, G. M.: High-resolution monthly rainfall database for Ethiopia: Homogenization,  
1107 reconstruction, and gridding, *J. Clim.*, 25, 8422-8443, 10.1175/jcli-d-12-00027.1,  
1108 2012.
- 1109 Uppala, S. M., K  llberg, P. W., Simmons, A. J., Andrae, U., Bechtold, V. D. C.,  
1110 Fiorino, M., Gibson, J. K., Haseler, J., Hernandez, A., Kelly, G. A., Li, X., Onogi, K.,  
1111 Saarinen, S., Sokka, N., Allan, R. P., Andersson, E., Arpe, K., Balmaseda, M. A.,  
1112 Beljaars, A. C. M., Berg, L. V. D., Bidlot, J., Bormann, N., Caires, S., Chevallier, F.,  
1113 Dethof, A., Dragosavac, M., Fisher, M., Fuentes, M., Hagemann, S., H  lm, E.,

1114 Hoskins, B. J., Isaksen, I., Janssen, P. A. E. M., Jenne, R., McNally, A. P., Mahfouf, J.  
1115 F., Morcrette, J. J., Rayner, N. A., Saunders, R. W., Simon, P., Sterl, A., Trenberth, K.  
1116 E., Untch, A., Vasiljevic, D., Viterbo, P., and Woollen, J.: The ERA-40 re-analysis, Q.  
1117 J. Roy. Meteorol. Soc., 131, 2961-3012, 10.1256/qj.04.176, 2005.

1118 Venema, V., Mestre, O., Aguilar, E., Auer, I., Guijarro, J., Domonkos, P., Vertacnik, G.,  
1119 Szentimrey, T., Stepanek, P., and Zahradnicek, P.: Benchmarking homogenization  
1120 algorithms for monthly data, *Clim. Past*, 8, 89-115, 2012.

1121 Wang, A., and Zeng, X.: Evaluation of multireanalysis products with in situ  
1122 observations over the Tibetan Plateau, *J. Geophys. Res. D Atmos.*, 117, D05102,  
1123 10.1029/2011JD016553, 2012.

1124 Wang, K., and Liang, S.: Global atmospheric downward longwave radiation over land  
1125 surface under all - sky conditions from 1973 to 2008, *J. Geophys. Res. D Atmos.*, 114,  
1126 D19101, 2009.

1127 Wang, K., Dickinson, R., Wild, M., and Liang, S.: Atmospheric impacts on climatic  
1128 variability of surface incident solar radiation, *Atmos. Chem. Phys.*, 12, 9581-9592,  
1129 2012.

1130 Wang, K., and Dickinson, R. E.: Global atmospheric downward longwave radiation at  
1131 the surface from ground-based observations, satellite retrievals, and reanalyses, *Rev.*  
1132 *Geophys.*, 51, 150-185, 10.1002/rog.20009, 2013.

1133 Wang, K.: Measurement biases explain discrepancies between the observed and  
1134 simulated decadal variability of surface incident solar radiation, *Sci. Rep.*, 4, 6144,  
1135 10.1038/srep06144, 2014.

1136 Wang, K. C., Ma, Q., Li, Z. J., and Wang, J. K.: Decadal variability of surface incident  
1137 solar radiation over China: Observations, satellite retrievals, and reanalyses, *J*  
1138 *Geophys Res-Atmos*, 120, 6500-6514, 10.1002/2015JD023420, 2015.

1139 Wang, X., and Wang, K.: Homogenized variability of radiosonde-derived atmospheric  
1140 boundary layer height over the global land surface from 1973 to 2014, *J. Clim.*, 29,  
1141 6893-6908, 10.1175/JCLI-D-15-0766.1, 2016.

1142 Wang, X. L., Wen, Q. H., and Wu, Y.: Penalized maximal t test for detecting  
1143 undocumented mean change in climate data series, *J. Appl. Meteor. Climatol.*, 46,  
1144 916-931, 2007.

1145 Wang, X. L.: Penalized maximal F test for detecting undocumented mean shift  
1146 without trend change, *J. Atmos. Oceanic Technol.*, 25, 368-384, 2008.

1147 Wang, X. L., Chen, H., Wu, Y., Feng, Y., and Pu, Q.: New techniques for the detection  
1148 and adjustment of shifts in daily precipitation data series, *J. Appl. Meteor. Climatol.*,  
1149 49, 2416-2436, 2010.



1150 Wang, X. L., and Feng, Y.: RHtestsV4 user manual, Atmospheric Science and  
 1151 Technology Directorate, Science and Technology Branch, Environment Canada. 28 pp.  
 1152 available at <http://etccdi.pacificclimate.org/software.shtml>, 2013.

1153 Wu, C., Chen, J. M., Pumpanen, J., Cescatti, A., Marcolla, B., Blanken, P. D., Ardö, J.,  
 1154 Tang, Y., Magliulo, V., and Georgiadis, T.: An underestimated role of precipitation  
 1155 frequency in regulating summer soil moisture, *Environ. Res. Lett.*, 7, 024011, 2012.

1156 Xu, J., and Powell, A. M., Jr.: Uncertainty of the stratospheric/tropospheric  
 1157 temperature trends in 1979-2008: multiple satellite MSU, radiosonde, and reanalysis  
 1158 datasets, *Atmos. Chem. Phys.*, 11, 10727-10732, 10.5194/acp-11-10727-2011, 2011.

1159 Yang, K., Koike, T., and Ye, B.: Improving estimation of hourly, daily, and monthly  
 1160 solar radiation by importing global data sets, *Agr. Forest Meteorol.*, 137, 43-55,  
 1161 10.1016/j.agrformet.2006.02.001, 2006.

1162 York, D., Evensen, N. M., Martínez, M. L., and Delgado, J. D. B.: Unified equations  
 1163 for the slope, intercept, and standard errors of the best straight line, *Am. J. Phys.*, 72,  
 1164 367-375, 10.1119/1.1632486, 2004.

1165 You, Q., Kang, S., Pepin, N., Flügel, W.-A., Yan, Y., Behrawan, H., and Huang, J.:  
 1166 Relationship between temperature trend magnitude, elevation and mean temperature  
 1167 in the Tibetan Plateau from homogenized surface stations and reanalysis data, *Global*  
 1168 *Planet. Change*, 71, 124-133, 10.1016/j.gloplacha.2010.01.020, 2010.

1169 Zeng, Z., Piao, S., Li, L. Z., Zhou, L., Ciais, P., Wang, T., Li, Y., Lian, X., Wood, E. F.,  
 1170 and Friedlingstein, P.: Climate mitigation from vegetation biophysical feedbacks  
 1171 during the past three decades, *Nature Clim. Change*, 7, 432-436, 2017.

1172 Zhao, T., Guo, W., and Fu, C.: Calibrating and evaluating reanalysis surface  
 1173 temperature error by topographic correction, *J. Clim.*, 21, 1440-1446,  
 1174 10.1175/2007jcli1463.1, 2008.

1175 Zhou, C., and Wang, K.: Land surface temperature over global deserts: means,  
 1176 variability and trends, *J. Geophys. Res. D Atmos.*, 121, 2016JD025410,  
 1177 10.1002/2016JD025410, 2016a.

1178 Zhou, C., and Wang, K.: Evaluation of surface fluxes in ERA-Interim using flux  
 1179 tower data, *J. Clim.*, 29, 1573-1582, 10.1175/JCLI-D-15-0523.1, 2016b.

1180 Zhou, C., and Wang, K.: Biological and environmental controls on evaporative  
 1181 fractions at ameriflux sites, *J. Appl. Meteor. Climatol.*, 55, 145-161,  
 1182 10.1175/JAMC-D-15-0126.1, 2016c.

1183 Zhou, C., and Wang, K.: Spatiotemporal divergence of the warming hiatus over land  
 1184 based on different definitions of mean temperature, *Sci. Rep.*, 6, 31789,  
 1185 10.1038/srep31789, 2016d.

1186 Zhou, C., and Wang, K.: Contrasting daytime and nighttime precipitation variability  
 1187 between observations and eight reanalysis products from 1979 to 2014 in China, J.  
 1188 Clim., 30, 6443-6464, 10.1175/JCLI-D-16-0702.1, 2017a.

1189 Zhou, C., and Wang, K.: Quantifying the sensitivity of precipitation to the long-term  
 1190 warming trend and interannual-decadal variation of surface air temperature over  
 1191 China, J. Clim., 30, 3687-3703, 10.1175/jcli-d-16-0515.1, 2017b.

1192 Zhou, C., Wang, K., and Ma, Q.: Evaluation of eight current reanalyses in simulating  
 1193 land surface temperature from 1979 to 2003 in China, J. Clim., 30, 7379-7398,  
 1194 10.1175/jcli-d-16-0903.1, 2017.

1195 Zhou, C., Wang, K., and Qi, D.: Attribution of the July 2016 extreme precipitation  
 1196 event over China's Wuhan, Bull. Am. Meteorol. Soc., 99, S107-S112, 2018.

1197

1198

1199 **Table 1.** Summary information on the twelve reanalysis products, including institution, model resolution, assimilation  
 1200 system, surface observations included associated with surface air temperatures, sea ice and sea surface temperatures  
 1201 (SSTs) and greenhouse gas (GHG) boundary conditions. The number in the parentheses in the Model Name column is the  
 1202 year of the version of the forecast model used. More details on each product can be found in the associated reference.

Reanalysis	Institution	Model Name	Model Resolution	Period	Assimilation System
ERA-Interim	ECMWF	IFS version Cy31r2 (2007)	T255 ~80 km, 60 levels	1979 onwards	4D-VAR
JRA-55	JMA	JMA operational numerical weather prediction system (2009)	T319 ~55 km, 60 levels	1958-2013	4D-VAR
NCEP-R1	NCEP/NCAR	NCEP operational numerical weather prediction system (1995)	T62 ~210 km, 28 levels	1948 onwards	3D-VAR
NCEP-R2	NCEP/DOE	Modified NCEP-R1 model (1998)	T62 ~210 km, 28 levels	1979 onwards	3D-VAR
MERRA	NASA/GMAO	GEOS-5.0.2 atmospheric general circulation model (2008)	0.5°× 0.667° ~55 km, 72 levels	1979 onwards	3D-VAR with incremental updating (GEOS IAU)
MERRA-2	NASA/GMAO	Updated version of GEOS-5.12.4 used in MERRA; its land model is similar to that of MERRA (2015)	0.5°× 0.625° ~55 km, 72 levels	1980 onwards	3D-VAR with incremental updating (GEOS IAU)
ERA-20C	ECMWF	IFS version Cy38r1 (2012), coupled atmosphere-land-ocean-waves system	T159 ~125 km, 91 levels	1900-2010	4D-VAR
ERA-20CM	ECMWF	Similar to that used in ERA-20C (2012)	T159 ~125 km, 91 levels	1900-2010	<del>3D-VAR</del>
CERA-20C	ECMWF	IFS version Cy41r2 (2016), coupled atmosphere-ocean-land-waves-sea ice system	T159 ~125 km, 91 levels	1901-2010	CERA ensemble assimilation technique
NOAA 20CRv2c	NOAA/ESRL PSD	NCEP GFS (2008), an updated version of the NCEP Climate Forecast System (CFS) coupled atmosphere-land model	T62 ~210 km, 28 levels	1851-2014	Ensemble Kalman filter
NOAA 20CRv2	NOAA/ESRL PSD	Same model as NOAA 20CRv2c (2008)	T62 ~210 km, 28 levels	1871-2012	Ensemble Kalman filter
CFSR	NCEP	NCEP CFS (2011) coupled atmosphere-ocean-land-sea ice model	T382 ~38 km, 64 levels	1979-2010	3D-VAR

Related Assimilated and Analysed Observations	Sea Ice and SSTs	GHG Forcing	Reference
1) Includes <i>in situ</i> observations of near-surface air temperature/pressure/relative humidity 2) Assimilates upper-air temperatures/wind/specific humidity 3) Assimilates rain-affected SSM/I radiances	A changing suite of SST and sea ice data from observations and NCEP	Interpolation by 1.6 ppmv/year from the global mean CO <sub>2</sub> in 1990 of 353 ppmv	(Dee et al., 2011b)
1) Analyses available near-surface observations 2) Assimilates all available traditional and satellite observations	<i>In situ</i> observation-based estimates of the COBE SST data and sea ice	Same as CMIP5	(Kobayashi et al., 2015)
1) Initiated with weather observations from ships, planes, station data, satellite observations and many more sources 2) No inclusion of near-surface air temperatures 3) Uses observed precipitation to nudge soil moisture 4) No information on aerosols	Reynolds SSTs for 1982 on and the UKMO GISST data for earlier periods; sea ice from SMMR/SSMI	Constant global mean CO <sub>2</sub> of 330 ppmv; no other trace gases	(Kalnay et al., 1996)
1) No inclusion of near-surface air temperatures 2) No information on aerosols	AMIP-II prescribed	Constant global mean CO <sub>2</sub> , 350 ppmv; no other trace gases	(Kanamitsu et al., 2002)
1) Neither MERRA nor MERRA-2 analyse near-surface air temperature, relative humidity, or other variables 2) Radiosondes do provide some low-level observations	Reynolds SSTs prescribed	Same as CMIP5	(Rienecker et al., 2011)
1) Includes newer observations (not included in MERRA) after the 2010s 2) Includes aerosols from MODIS and AERONET measurements over land after the 2000s and from the GOCART model before the 2000s 3) Assimilates observation-corrected precipitation to correct the model-generated precipitation before reaching the land surface	AMIP-II and Reynolds SSTs	Same as CMIP5	(Reichle et al., 2017)
1) Assimilates surface pressures from ISPDv3.2.6 and ICOADSv2.5.1 and surface marine winds from ICOADSv2.5.1 2) Uses monthly climatology of aerosols from CMIP5	SSTs and sea ice from HadISST2.1.0.0	Same as CMIP5	(Poli et al., 2016)
Assimilates no data and includes radiative forcings from CMIP5	SSTs and sea ice realizations from HadISST2.1.0.0 used in 10 members	Same as CMIP5	(Hersbach et al., 2015)
1) Assimilates surface pressures from ISPDv3.2.6 and ICOADSv2.5.1 and surface marine winds from ICOADSv2.5.1 2) Assimilates no data in the land, wave and sea ice components but uses the coupled model at each time step	SSTs from HadISST2.1.0.0	Same as CMIP5	(Laloyaux et al., 2016)
Assimilates only surface pressure and sea level pressure	SSTs from HadISST1.1 and sea ice from COBE SST	Monthly 15° gridded estimates of CO <sub>2</sub> from WMO observations	(Compo et al., 2011)
Same as NOAA 20CRv2c	SSTs and sea ice from HadISST1.1	Monthly 15° gridded estimates of CO <sub>2</sub> from WMO observations	(Compo et al., 2011)
1) Assimilates all available conventional and satellite observations but not near-surface air temperatures 2) Atmospheric model contains observed changes in aerosols 3) Uses observation-corrected precipitation to force the land surface analysis	Generated by coupled ocean-sea ice models; evolves freely during the 6-h coupled model integration	Monthly 15° gridded estimates of CO <sub>2</sub> from WMO observations	(Saha et al., 2010)

**Table 2.** Differences (unit: °C) relative to the homogenized observations and trends (unit: °C/decade) in surface air temperatures ( $T_a$ ) from 1979 to 2010 over China and its seven subregions. The bold and italic bold fonts indicate results that are significant according to two-tailed Student’s  $t$ -tests with significance levels of 0.05 and 0.1, respectively.

Region	China		Tibetan Plateau		Northwest China		Loess Plateau		Middle China		Northeast China		North China Plain		Southeast China	
	Diff.	Trend	Diff.	Trend	Diff.	Trend	Diff.	Trend	Diff.	Trend	Diff.	Trend	Diff.	Trend	Diff.	Trend
ERA-Interim	-0.87	<b>0.38</b>	-3.49	<b>0.33</b>	-1.82	<b>0.37</b>	-0.32	<b>0.50</b>	-1.19	<b>0.28</b>	-0.03	<b>0.42</b>	-0.02	<b>0.45</b>	-0.03	<b>0.37</b>
NCEP-R1	-2.56	<b>0.23</b>	-6.80	0.11	-4.45	<b>0.39</b>	-1.77	<b>0.21</b>	-2.91	<b>0.23</b>	-1.28	<b>0.27</b>	-1.21	<b>0.23</b>	-1.33	<b>0.22</b>
MERRA	-0.48	<b>0.25</b>	-3.48	<b>0.33</b>	0.95	0.14	1.14	0.09	-1.35	<b>0.12</b>	-0.22	<b>0.52</b>	0.67	<b>0.26</b>	-0.27	<b>0.24</b>
JRA-55	-1.10	<b>0.38</b>	-3.49	<b>0.42</b>	-1.70	<b>0.39</b>	-0.58	<b>0.52</b>	-1.61	<b>0.30</b>	-0.25	<b>0.37</b>	-0.26	<b>0.41</b>	-0.50	<b>0.34</b>
NCEP-R2	-2.10	<b>0.25</b>	-5.76	-0.07	-4.29	<b>0.58</b>	-1.33	0.10	-2.80	<b>0.20</b>	-0.51	<b>0.36</b>	-0.38	<b>0.23</b>	-1.14	<b>0.36</b>
MERRA2	-0.91	<b>0.28</b>	-3.41	<b>0.35</b>	0.34	<b>0.32</b>	0.12	<b>0.19</b>	-1.35	<b>0.23</b>	-0.73	<b>0.41</b>	-0.24	0.18	-0.64	<b>0.25</b>
ERA-20C	-1.42	<b>0.29</b>	-6.56	<b>0.33</b>	-1.95	<b>0.31</b>	0.03	0.21	-2.01	<b>0.35</b>	-0.19	<b>0.32</b>	1.05	0.19	-0.47	<b>0.28</b>
ERA-20CM	-1.48	<b>0.32</b>	-5.93	<b>0.28</b>	-1.39	<b>0.38</b>	-0.36	<b>0.33</b>	-2.13	<b>0.27</b>	-0.23	<b>0.41</b>	-0.31	<b>0.34</b>	-0.51	<b>0.29</b>
CERA-20C	-2.06	<b>0.34</b>	-7.00	<b>0.41</b>	-2.15	<b>0.38</b>	-0.78	<b>0.36</b>	-2.59	<b>0.34</b>	-0.76	<b>0.43</b>	-0.40	0.19	-1.20	<b>0.29</b>
NOAA 20CRv2c	-0.28	<b>0.22</b>	-2.75	<b>0.39</b>	-0.01	<b>0.28</b>	1.62	0.16	-1.68	<b>0.18</b>	-0.16	0.11	1.06	0.15	0.18	<b>0.22</b>
NOAA 20CRv2	-0.32	<b>0.24</b>	-2.78	<b>0.33</b>	-0.01	<b>0.29</b>	1.48	0.20	-1.77	<b>0.19</b>	-0.07	0.25	0.97	0.21	0.12	<b>0.19</b>
CFSR	-1.74	<b>0.48</b>	-5.09	<b>0.46</b>	-1.03	<b>0.44</b>	-0.25	<b>0.40</b>	-2.91	<b>0.37</b>	-0.49	<b>0.67</b>	-0.37	<b>0.47</b>	-1.58	<b>0.51</b>
Obs-raw	0.03	<b>0.40</b>	0.03	<b>0.46</b>	0.09	<b>0.44</b>	0.01	<b>0.52</b>	0.05	<b>0.30</b>	0.00	<b>0.40</b>	0.05	<b>0.42</b>	0.03	<b>0.36</b>
Obs-homogenized		<b>0.37</b>		<b>0.44</b>		<b>0.36</b>		<b>0.50</b>		<b>0.24</b>		<b>0.41</b>		<b>0.38</b>		<b>0.33</b>

1209 **Table 3.** Spatial pattern correlation (unit: 1) of three groups: partial relationships, trends and simulated biases in the trends in  
 1210 surface air temperature ( $T_a$ ) against surface incident solar radiation ( $R_s$ ), precipitation frequency (PF) and surface downward  
 1211 longwave radiation ( $L_d$ ). The bold and italic bold fonts indicate results that are significant according to two-tailed Student's  
 1212 t-tests with significance levels of 0.05 and 0.1, respectively.

Pattern Correlation	Partial Relationship						Trend				Trend Bias		
	$(T_a, R_s)$		$(T_a, \text{PF})$		$(T_a, L_d)$		$(T_a, T_a)$	$(T_a, R_s)$	$(T_a, \text{PF})$	$(T_a, L_d)$	$(T_a, R_s)$	$(T_a, \text{PF})$	$(T_a, L_d)$
	Corr.	Slope	Corr.	Slope	Corr.	Slope							
ERA-Interim	<b>0.29</b>	0.01	0.03	<b>0.31</b>	<b>0.21</b>	<b>0.25</b>	<b>0.47</b>	<b>-0.11</b>	-0.04	<b>0.33</b>	<b>0.26</b>	<b>-0.12</b>	<b>0.10</b>
NCEP-R1	<b>0.30</b>	<i>0.06</i>	<b>0.18</b>	<b>0.30</b>	<b>0.36</b>	0.00	0.02	<b>-0.36</b>	-0.02	<b>0.62</b>	-0.03	-0.04	<b>0.43</b>
MERRA	<b>0.29</b>	0.06	<b>0.13</b>	<b>0.39</b>	0.05	<b>0.20</b>	<b>0.21</b>	<b>0.66</b>	<b>-0.81</b>	<b>-0.53</b>	<b>0.42</b>	<b>-0.62</b>	-0.05
JRA-55	<b>0.35</b>	<b>0.21</b>	<b>0.22</b>	<b>0.16</b>	<b>0.29</b>	<b>0.27</b>	<b>0.54</b>	<b>-0.33</b>	<b>0.31</b>	<b>0.57</b>	0.00	<b>0.14</b>	<b>0.29</b>
NCEP-R2	<b>0.22</b>	0.03	<b>0.20</b>	<b>0.36</b>	<b>0.27</b>	0.04	<b>-0.08</b>	<b>0.18</b>	<b>-0.29</b>	<b>0.28</b>	<b>0.15</b>	<b>-0.14</b>	<b>0.35</b>
MERRA2	<b>0.13</b>	0.05	<b>0.26</b>	<b>0.43</b>	<b>0.09</b>	<b>0.30</b>	<b>0.22</b>	<b>0.30</b>	<b>-0.11</b>	<b>0.11</b>	-0.02	<b>-0.12</b>	<b>0.28</b>
ERA-20C	<b>0.28</b>	<b>-0.07</b>	<b>-0.07</b>	<b>0.43</b>	<b>0.19</b>	0.02	-0.07	<b>0.18</b>	<b>-0.33</b>	0.03	<b>0.11</b>	<b>-0.25</b>	<b>0.31</b>
ERA-20CM	<b>0.24</b>	-0.04	-0.03	<b>0.32</b>	<b>0.26</b>	<b>0.18</b>	<b>0.28</b>	<b>-0.32</b>	<b>0.31</b>	<b>0.83</b>	-0.02	<b>0.12</b>	<b>0.34</b>
CERA-20C	<b>0.41</b>	<b>0.17</b>	<b>0.10</b>	<b>0.37</b>	<b>0.08</b>	<i>0.07</i>	<b>0.29</b>	<b>0.50</b>	<b>-0.58</b>	<b>-0.07</b>	-0.01	<b>-0.22</b>	<b>0.23</b>
NOAA 20CRv2c	<b>0.39</b>	<b>0.15</b>	<b>-0.22</b>	<b>0.25</b>	<b>0.14</b>	<b>0.15</b>	<b>0.08</b>	<b>-0.07</b>	<b>-0.11</b>	<b>0.55</b>	<b>-0.25</b>	<b>-0.05</b>	<b>0.50</b>
NOAA 20CRv2	<b>0.38</b>	<b>0.15</b>	<b>-0.21</b>	<b>0.18</b>	<b>0.14</b>	<b>0.23</b>	<b>0.19</b>	-0.02	<b>-0.20</b>	<b>0.56</b>	<b>-0.18</b>	<b>0.11</b>	<b>0.47</b>
CFSR	<b>0.33</b>	<b>0.12</b>	<b>0.10</b>	<b>0.19</b>	<b>0.37</b>	<b>0.21</b>	<b>0.19</b>	<b>0.11</b>	<b>-0.26</b>	<b>0.07</b>	<b>0.31</b>	<b>-0.08</b>	<b>0.15</b>
Obs-raw								<b>-0.07</b>	<b>0.27</b>	<b>0.50</b>			
Obs-homogenized								<b>-0.09</b>	<b>0.35</b>	<b>0.32</b>			

**Figure Captions:**

**Figure 1.** The multiyear-averaged differences in surface air temperatures ( $T_a$ , unit: °C) during the period of 1979-2010 from the twelve reanalysis products relative to the homogenized observations over China. The reanalysis products are (a) ERA-Interim, (b) NCEP-R1, (c) MERRA, (d) JRA-55, (e) NCEP-R2, (f) MERRA2, (g) ERA-20C, (h) ERA-20CM, (i) CERA-20C, (j) NOAA 20CRv2c, (k) NOAA 20CRv2 and (l) CFSR. The mainland of China is divided into seven regions (shown in Fig. 1c), specifically ① the Tibetan Plateau, ② Northwest China, ③ the Loess Plateau, ④ Middle China, ⑤ Northeast China, ⑥ the North China Plain and ⑦ South China.

**Figure 2.** The impact of inconsistencies between station and model elevations on the simulated multiyear-averaged differences in surface air temperatures ( $T_a$ , unit: °C) during the study period of 1979-2010 over China. The elevation difference ( $\Delta\text{Height}$ ) between the stations and the models consists of the filtering error in the elevations used in the spectral models ( $\Delta f$ ) and the difference in site-to-grid elevations ( $\Delta s$ ) due to the complexity of orographic topography.  $\Delta f$  is derived from the model elevations minus the ‘true’ elevations in the corresponding model grid cells from GTOPO30. The GTOPO30 orography is widely used in reanalyses, e.g., by ECMWF. The colour bar denotes the station elevations (unit: m). The relationship of the  $T_a$  differences is regressed on  $\Delta\text{Height}$  (shown at the bottom of each subfigure) or  $\Delta f$  and  $\Delta s$  (shown at the top of each subfigure); the corresponding explained variances are shown.

**Figure 3.** Taylor diagrams for annual time series of the observed and reanalysed surface air temperature anomalies ( $T_a$ , unit: °C) from 1979 to 2010 in (a) China and

(b-h) the seven subregions. The correlation coefficient, standard deviation and root mean squared error (RMSE) are calculated against the observed homogenized  $T_a$  anomalies.

**Figure 4.** Composite map of partial correlation coefficients of the detrended surface air temperature ( $T_a$ , unit: °C) against surface incident solar radiation ( $R_s$ ), precipitation frequency (PF) and surface downward longwave radiation ( $L_d$ ) during the period of 1979-2010 from observations and the twelve reanalysis products. The marker ‘+’ denotes the negative partial correlations of  $T_a$  with  $R_s$  over the Tibetan Plateau in NCEP-R2, ERA-20C and ERA-20CM.

**Figure 5. (a, b)** The observed trends in surface air temperature ( $T_a$ , unit: °C/decade) and the simulated biases in the trends in  $T_a$  (unit: °C/decade) during the period of 1979-2010 from (c) raw observations and (d-o) the twelve reanalysis products over China with respect to the homogenized observations. The squares denote the original homogeneous time series, and the dots denote the adjusted homogeneous time series. The probability distribution functions of all of the biases in the trends are shown as coloured histograms, and the black stairs are integrated from the trend biases with a significance level of 0.05 (based on two-tailed Student’s  $t$ -tests). The cyan and green stars in (k-n) represent estimates of the biases in the trends outside the ensemble ranges whose locations are denoted by the black dots shown in (k-n).

**Figure 6.** Composite map of the contributions (unit: °C/decade) of the biases in the trends in three relevant parameters, surface incident solar radiation ( $R_s$ , in red), surface downward longwave radiation ( $L_d$ , in green) and precipitation frequency (in



blue) to the biases in the trends in surface air temperature ( $T_a$ ) during the study period of 1979-2010, as estimated using the twelve reanalysis products over China.

**Figure 7.** Contributions (unit: °C/decade) of the biases in the trends in surface air temperatures ( $T_a$ ) from three relevant parameters, surface incident solar radiation ( $R_s$ , in brown), surface downward longwave radiation ( $L_d$ , in light blue) and precipitation frequency (PF, in deep blue) during the study period of 1979-2010 from the twelve reanalysis products over China and its seven subregions.

**Figure 8.** Spatial associations of the simulated biases in the trend in surface air temperature ( $T_a$ ) versus three relevant parameters among the twelve reanalysis products (solid lines indicate the NWP-like reanalyses, and dashed lines indicate the climate reanalyses). The probability density functions (unit: %) of these biases in the trends are estimated from approximately 700 1°×1° grid cells that cover China. The median values (coloured dots with error bars of spatial standard deviations) of the biases in the trends in  $T_a$  (unit: °C/decade) in the twelve reanalyses are regressed onto those of (a) the surface incident solar radiation ( $R_s$ , unit: W·m<sup>-2</sup>/decade), (b) precipitation frequency (unit: days/decade) and (c) the surface downward longwave radiation ( $L_d$ , unit: W·m<sup>-2</sup>/decade) using the ordinary least squares method (OLS, denoted by the dashed grey lines) and the weighted total least squares method (WTLS, denoted by the solid black lines). The 5-95% confidence intervals of the regressed slopes obtained using WTLS are shown as shading. The regressed correlations and slopes are shown as grey and black text, respectively.

# NWP-like reanalysis

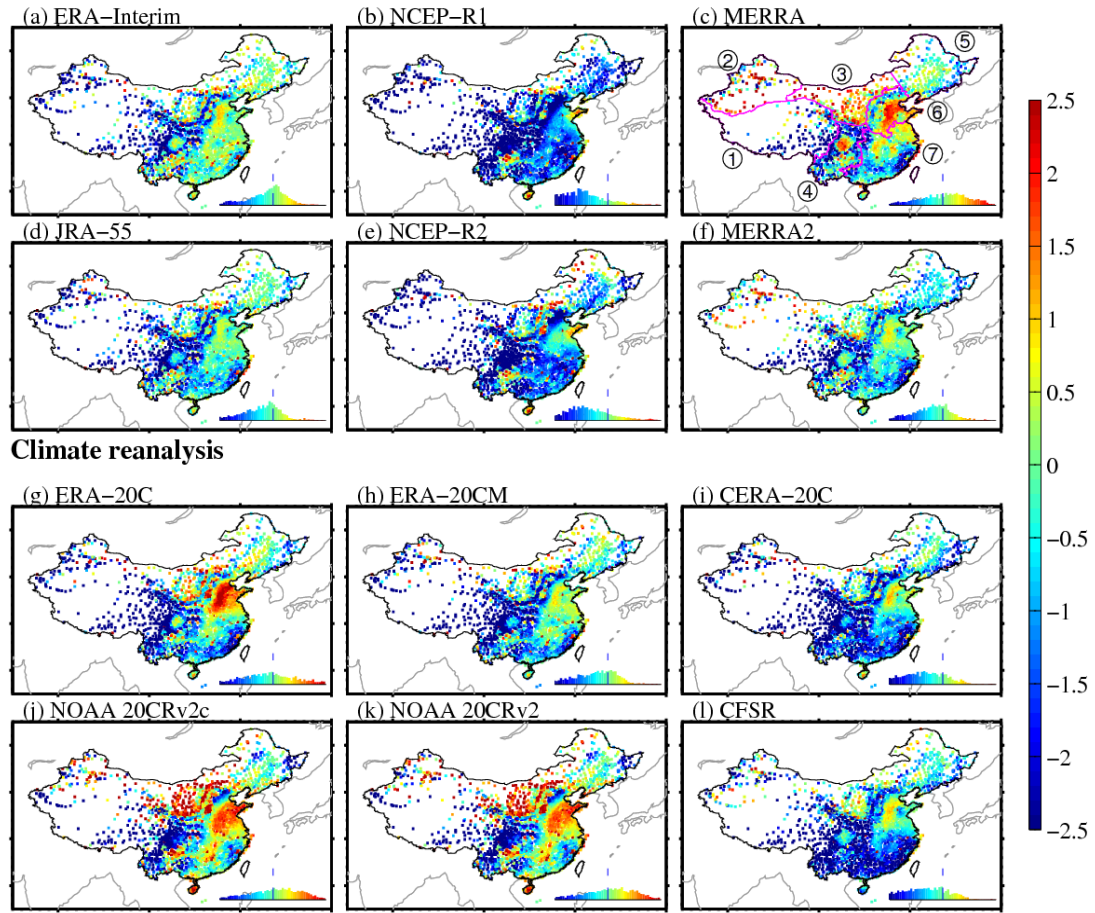


**Figure 1.** The multiyear-averaged differences in surface air temperatures ( $T_a$ , unit:  $^{\circ}\text{C}$ ) during the period of 1979-2010 from the twelve reanalysis products relative to the homogenized observations over China. The reanalysis products are (a) ERA-Interim, (b) NCEP-R1, (c) MERRA, (d) JRA-55, (e) NCEP-R2, (f) MERRA2, (g) ERA-20C, (h) ERA-20CM, (i) CERA-20C, (j) NOAA 20CRv2c, (k) NOAA 20CRv2 and (l) CFSR. The mainland of China is divided into seven regions (shown in Fig. 1c), specifically ① the Tibetan Plateau, ② Northwest China, ③ the Loess Plateau, ④ Middle China, ⑤ Northeast China, ⑥ the North China Plain and ⑦ South China.

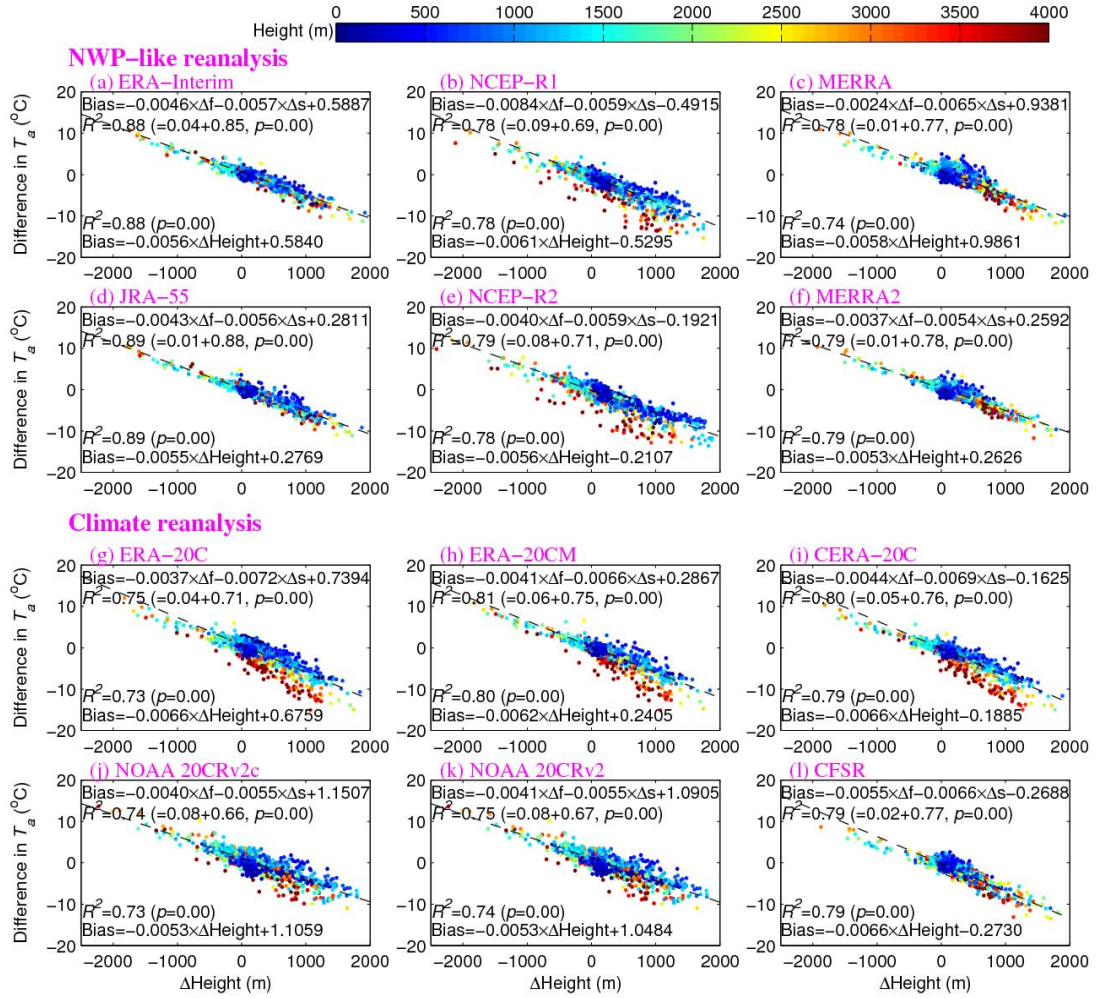


**Figure 2.** The impact of inconsistencies between station and model elevations on the simulated multiyear-averaged differences in surface air temperatures ( $T_a$ , unit:  $^{\circ}\text{C}$ ) during the study period of 1979-2010 over China. The elevation difference ( $\Delta\text{Height}$ ) between the stations and the models consists of the filtering error in the elevations used in the spectral models ( $\Delta f$ ) and the difference in site-to-grid elevations ( $\Delta s$ ) due to the complexity of orographic topography.  $\Delta f$  is derived from the model elevations minus the ‘true’ elevations in the corresponding model grid cells from GTOPO30. The GTOPO30 orography is widely used in reanalyses, e.g., by ECMWF. The colour bar denotes the station elevations (unit: m). The relationship of the  $T_a$  differences is regressed on  $\Delta\text{Height}$  (shown at the bottom of each subfigure) or  $\Delta f$  and  $\Delta s$  (shown at

1298 the top of each subfigure); the corresponding explained variances are shown.

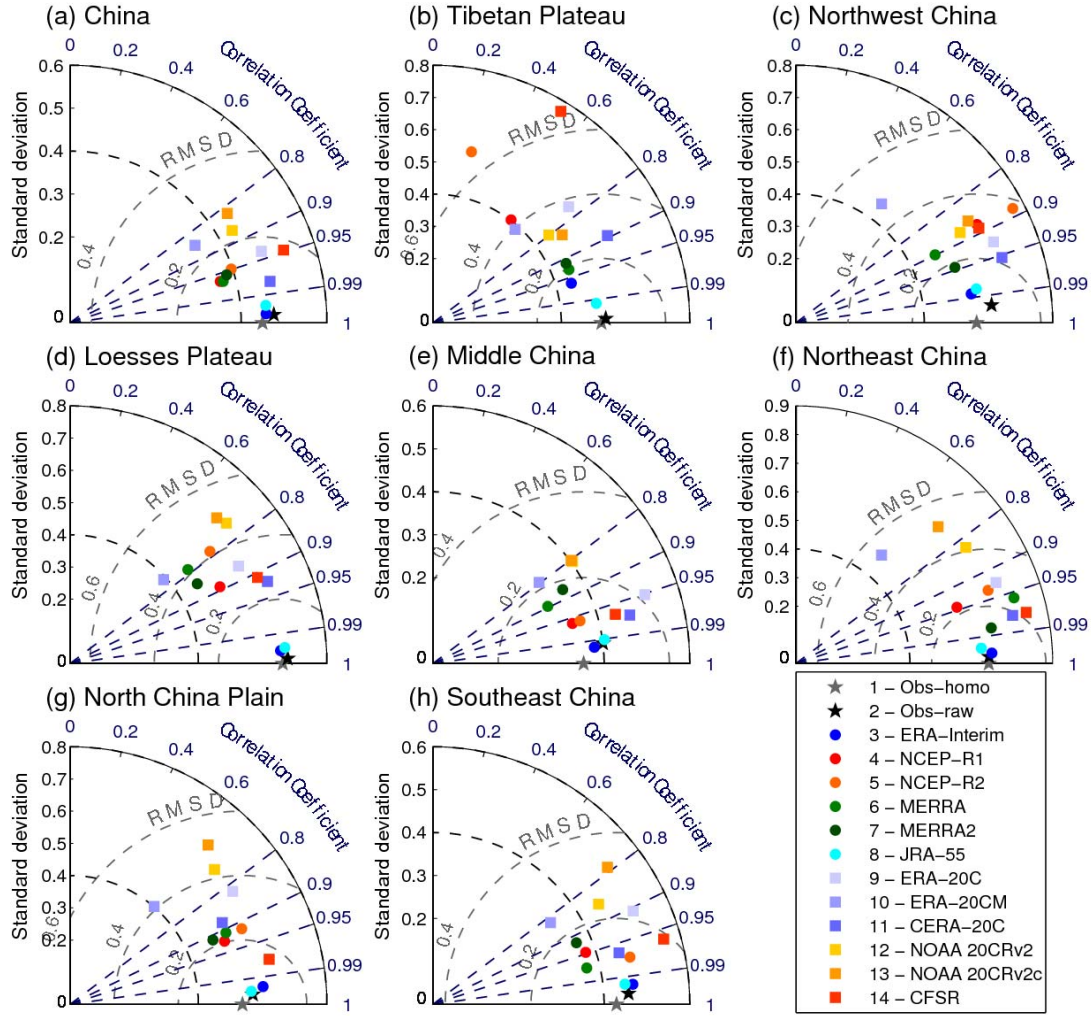


**Figure 3.** Taylor diagrams for annual time series of the observed and reanalysed surface air temperature anomalies ( $T_a$ , unit:  $^{\circ}\text{C}$ ) from 1979 to 2010 in (a) China and (b-h) the seven subregions. The correlation coefficient, standard deviation and root mean squared error (RMSE) are calculated against the observed homogenized  $T_a$  anomalies.



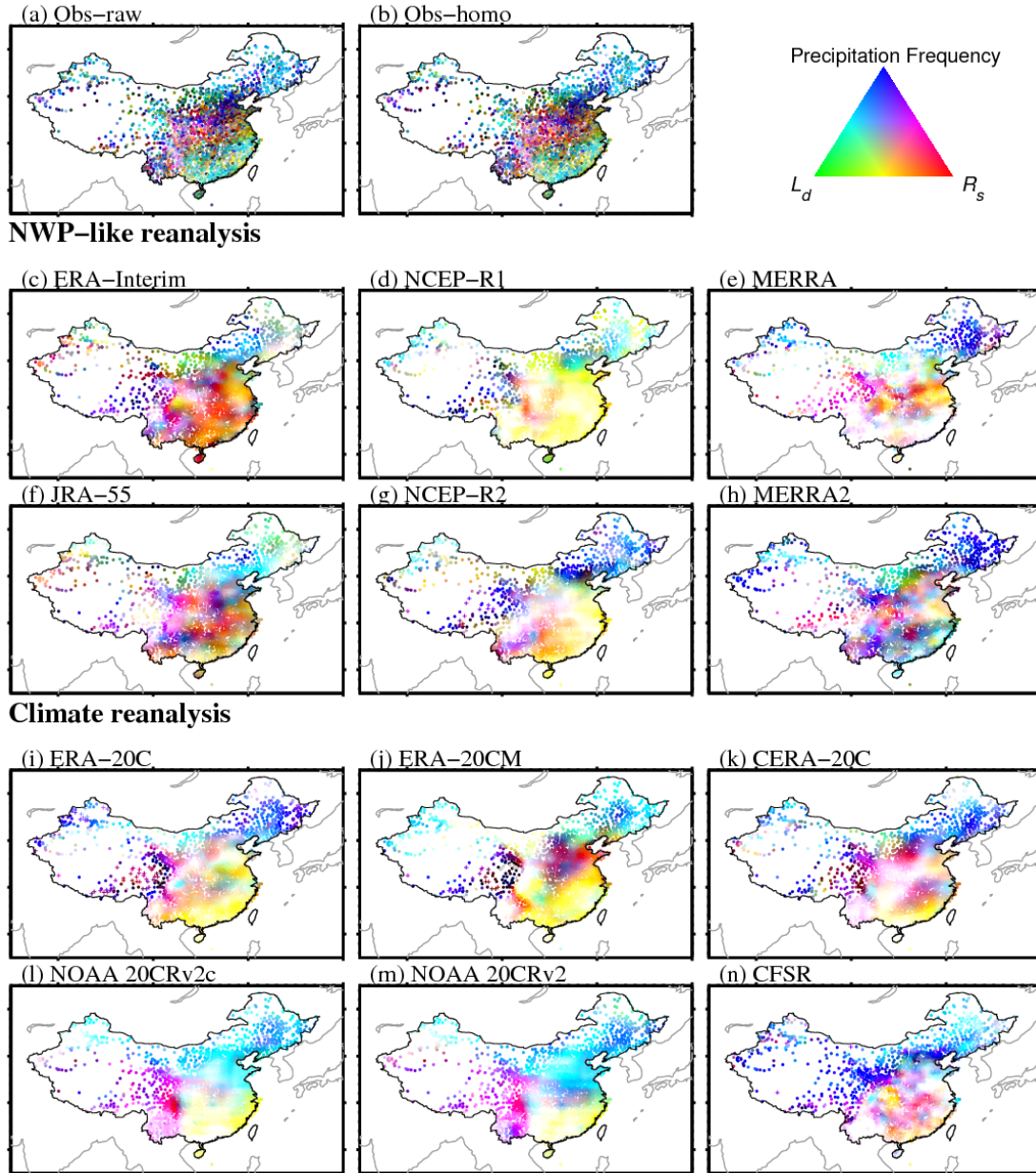


**Figure 4.** Composite map of partial correlation coefficients of the detrended surface air temperature ( $T_a$ , unit:  $^{\circ}\text{C}$ ) against surface incident solar radiation ( $R_s$ ), precipitation frequency (PF) and surface downward longwave radiation ( $L_d$ ) during the period of 1979-2010 from observations and the twelve reanalysis products. The marker ‘+’ denotes the negative partial correlations of  $T_a$  with  $R_s$  over the Tibetan Plateau in NCEP-R2, ERA-20C and ERA-20CM.

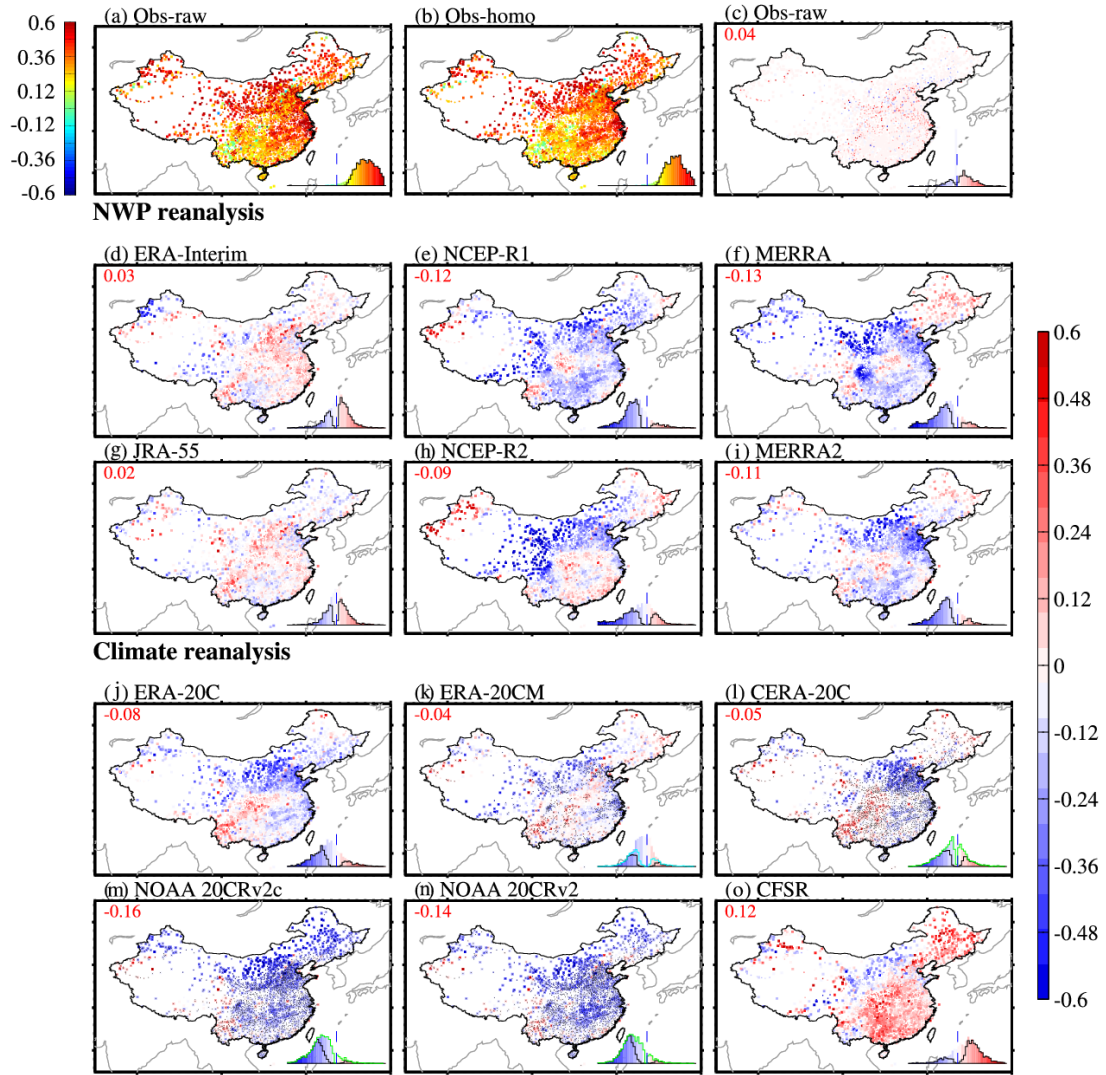


**Figure 5.** (a, b) The observed trends in surface air temperature ( $T_a$ , unit:  $^{\circ}\text{C}/\text{decade}$ ) and the simulated biases in the trends in  $T_a$  (unit:  $^{\circ}\text{C}/\text{decade}$ ) during the period of 1979-2010 from (c) raw observations and (d-o) the twelve reanalysis products over China with respect to the homogenized observations. The squares denote the original homogeneous time series, and the dots denote the adjusted homogeneous time series. The probability distribution functions of all of the biases in the trends are shown as coloured histograms, and the black stairs are integrated from the trend biases with a significance level of 0.05 (based on two-tailed Student's  $t$ -tests). The cyan and green stars in (k-n) represent estimates of the biases in the trends outside the ensemble

1322 ranges whose locations are denoted by the black dots shown in (k-n).



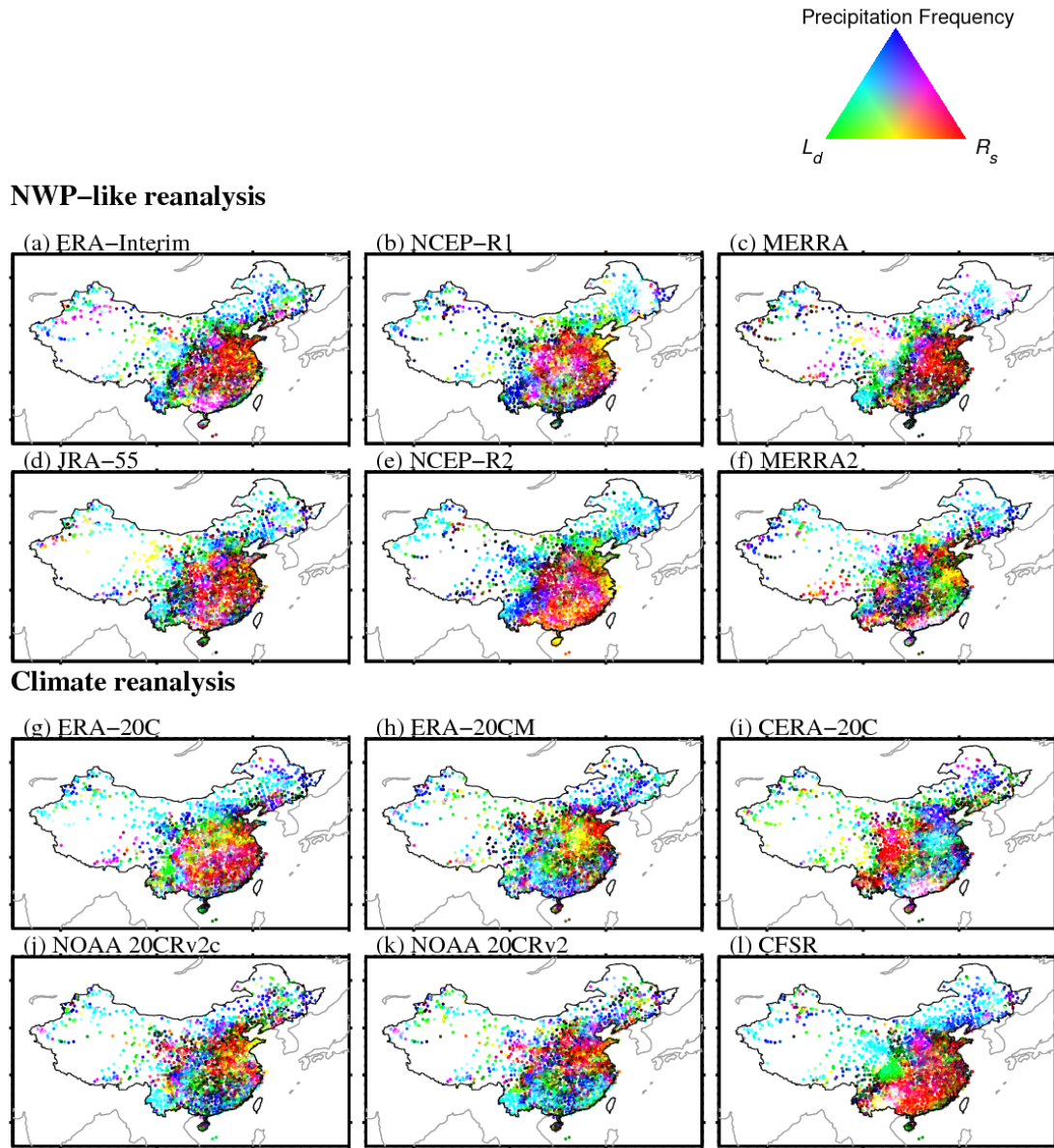


**Figure 6.** Composite map of the contributions (unit: °C/decade) of the biases in the trends in three relevant parameters, surface incident solar radiation ( $R_s$ , in red), surface downward longwave radiation ( $L_d$ , in green) and precipitation frequency (in blue) to the biases in the trends in surface air temperature ( $T_a$ ) during the study period of 1979-2010, as estimated using the twelve reanalysis products over China.

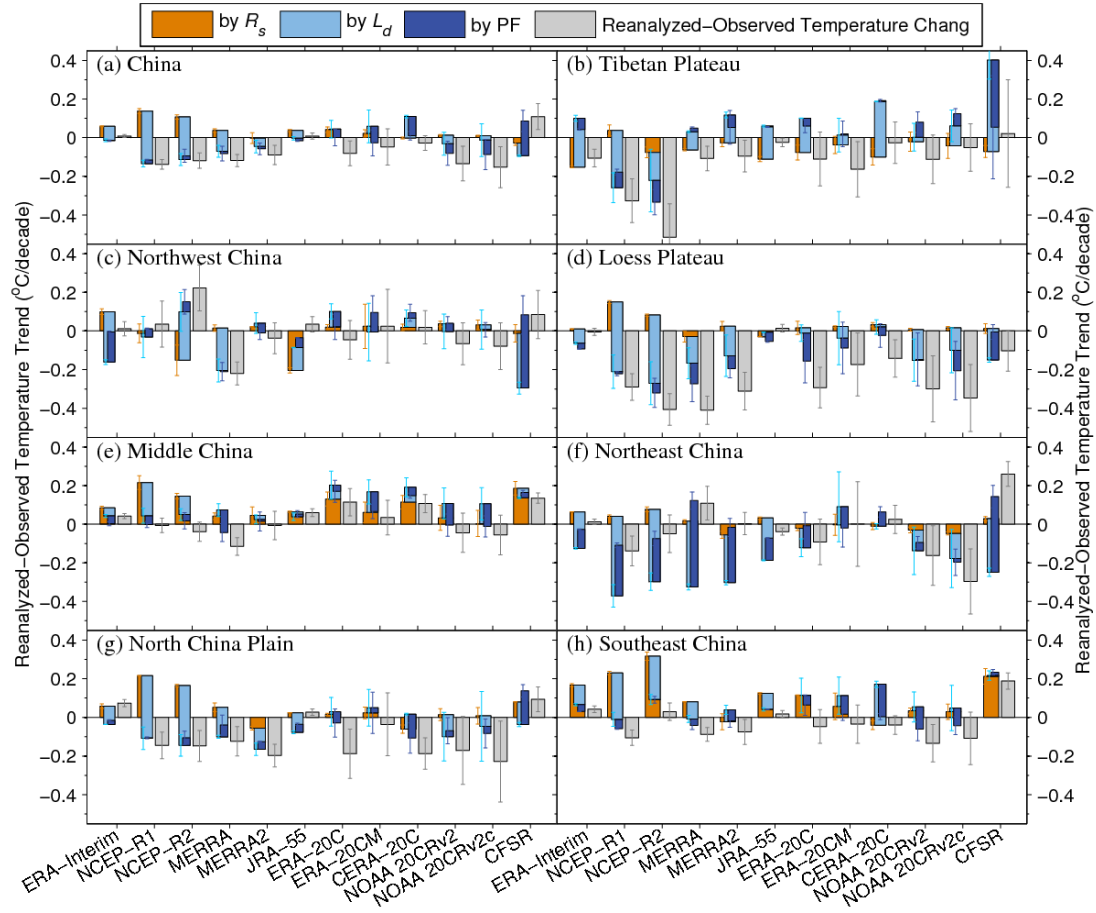


**Figure 7.** Contribution s(unit: °C/decade) of the biases in the trends in surface air temperatures ( $T_a$ ) from three relevant parameters, surface incident solar radiation ( $R_s$ , in brown), surface downward longwave radiation ( $L_d$ , in light blue) and precipitation frequency (PF, in deep blue) during the study period of 1979-2010 from the twelve reanalysis products over China and its seven subregions.

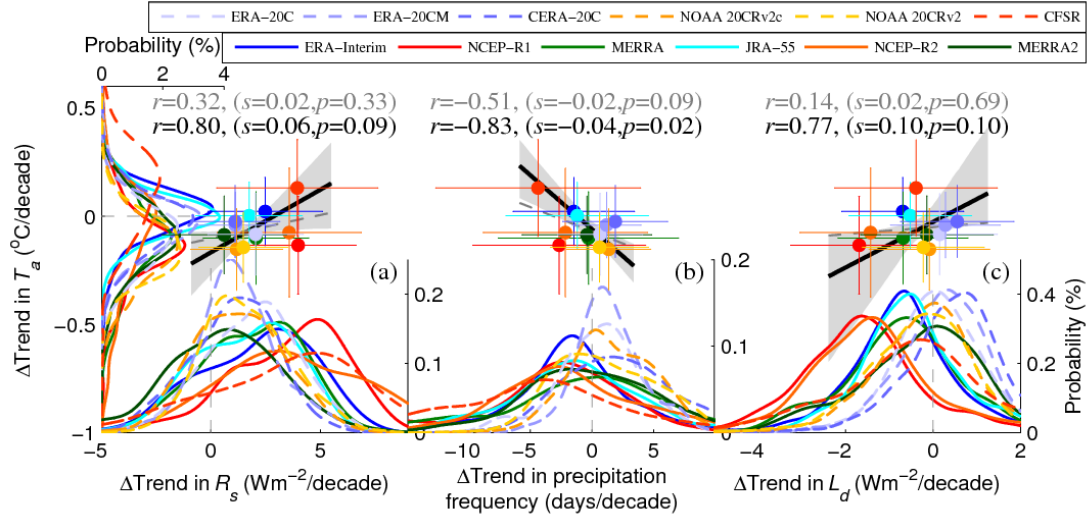


**Figure 8.** Spatial associations of the simulated biases in the trend in surface air temperature ( $T_a$ ) versus three relevant parameters among the twelve reanalysis products (solid lines indicate the NWP-like reanalyses, and dashed lines indicate the climate reanalyses). The probability density functions (unit: %) of these biases in the trends are estimated from approximately 700  $1^\circ \times 1^\circ$  grid cells that cover China. The median values (coloured dots with error bars of spatial standard deviations) of the biases in the trends in  $T_a$  (unit:  $^\circ\text{C}/\text{decade}$ ) in the twelve reanalyses are regressed onto those of (a) the surface incident solar radiation ( $R_s$ , unit:  $\text{W}\cdot\text{m}^{-2}/\text{decade}$ ), (b) precipitation frequency (unit: days/decade) and (c) the surface downward longwave radiation ( $L_d$ , unit:  $\text{W}\cdot\text{m}^{-2}/\text{decade}$ ) using the ordinary least squares method (OLS, denoted by the dashed grey lines) and the weighted total least squares method (WTLS, denoted by the solid black lines). The 5-95% confidence intervals of the regressed slopes obtained using WTLS are shown as shading. The regressed correlations and slopes are shown as grey and black text, respectively.